AD_____

Award Number: W81XWH-07-1-0547

TITLE: Imaging of Ep-CAM Positive Metastatic Cancer in the Lymph System

PRINCIPAL INVESTIGATOR: Dr. Kristen Adams

CONTRACTING ORGANIZATION: University of Texas Health Science Center
Houston, TX 77030

REPORT DATE: January 2011

TYPE OF REPORT: Final

PREPARED FOR: U.S. Army Medical Research and Materiel Command
Fort Detrick, Maryland 21702-5012

REPORT DOCUMENTATION PAGE

Form Approved
OMB No. 0704-0188

1. REPORT DATE *(DD-MM-YYYY)*	**2. REPORT TYPE**	**3. DATES COVERED** *(From - To)*
01-01-2011	Final	15 Aug 2007 - 29 DEC 2010

4. TITLE AND SUBTITLE

Imaging of Ep-CAM Positive Metastatic Cancer in the Lymph System

5a. CONTRACT NUMBER

5b. GRANT NUMBER
W81XWH-07-1-0547

5c. PROGRAM ELEMENT NUMBER

6. AUTHOR(S)
Dr. Kristen Adams

E-Mail: keadams@gmail.com

5d. PROJECT NUMBER

5e. TASK NUMBER

5f. WORK UNIT NUMBER

7. PERFORMING ORGANIZATION NAME(S) AND ADDRESS(ES)
University of Texas Health Science Center
Houston, TX 77030

8. PERFORMING ORGANIZATION REPORT NUMBER

9. SPONSORING / MONITORING AGENCY NAME(S) AND ADDRESS(ES)
U.S. Army Medical Research and Materiel Command
Fort Detrick, Maryland 21702-5012

10. SPONSOR/MONITOR'S ACRONYM(S)

11. SPONSOR/MONITOR'S REPORT NUMBER(S)

12. DISTRIBUTION / AVAILABILITY STATEMENT
Approved for Public Release; Distribution Unlimited

13. SUPPLEMENTARY NOTES

14. ABSTRACT

The majority of cancer mortalities occur not from the primary tumor but rather from distant metastases. Since the lymphatic system provides a route for the spread of metastatic cancer cells, it is not surprising that lymph node status serves as the primary prognostic indicator in most cancers. This work aims to improve the methodology for and accuracy of diagnosing cancer positive lymph nodes. Better diagnoses could increase survival by detecting more true positive nodes which can then be removed while reducing adverse affects by correctly identifying the negative nodes which can be retained and should contribute to improved overall lymph function.

15. SUBJECT TERMS

No subject terms provided.

16. SECURITY CLASSIFICATION OF:			**17. LIMITATION OF ABSTRACT**	**18. NUMBER OF PAGES**	**19a. NAME OF RESPONSIBLE PERSON**
a. REPORT	**b. ABSTRACT**	**c. THIS PAGE**			USAMRMC
U	U	U	UU	38	**19b. TELEPHONE NUMBER** *(include area code)*

Table of Contents

Introduction

The majority of cancer mortalities occur not from the primary tumor but rather from distant metastases. Since the lymphatic system provides a route for the metastatic spread of cancer, it is not surprising that lymph node status serves as the primary prognostic indicator in most cancers. Currently, occult lymph node staging requires surgical removal of lymph nodes for subsequent biopsy, which in itself has significant morbidity. Specifically, in the case of breast cancer, axillary node resection is associated with an elevated risk of breast cancer-related lymphedema. This research plan aims to develop a unique imaging agent to identify metastatic tumor cells within the lymph nodes of cancer patients, initially with breast cancer patients. Development of a non-invasive methodology for nodal staging could eventually enable surgeons to intra-operatively differentiate cancer positive and negative lymph nodes, allowing for the specific resection of positive nodes and retention of cancer negative nodes.

The project includes development of a new imaging agent based on anti-Ep-CAM antibody and preclinical testing of the binding and pharmacokinetics with the eventual goal of clinical translation. In achieving these goals, I will (i) modify an established humanized antibody against the epithelial cell adhesion molecule (Ep-CAM) by dual-labeling with a near infrared (NIR) fluorescent dye and a radiotracer to image epithelial cell based cancers in the lymph compartment with optical and nuclear imaging modalities; (ii) deliver low doses of the imaging agent directly into the lymphatic space; and (iii) develop a custom gain-modulated intensified camera for intraoperative optical lymph imaging.

Body

Preclinical Ep-Cam Imaging Studies

Phase I of the preclinical Ep-CAM imaging studies included binding affinity studies, antibody labeling, HPLC validation, stability studies, testing of the affinity of dual-labeled antibody, and specificity (blocking) assays.

An antibody against the human epithelial cell adhesion molecule (Ep-CAM) and the control immunoglobulin gamma were purchased from RnD Biosystems (Minneapolis, MN). Antibodies were covalently coupled to IRDye 800CW-NHS Ester from Licor, Inc, (Lincoln, NE). The conjugation ratio was 1.5 to 2.8 IRDye molecules per antibody. The retention of specific binding ability of anti-Ep-CAM-IR800 was tested using two human breast cancer cell lines, MT3 and SKBr3. SKBr3 cells (ATCC, Manassas, VA) express low levels of Ep-CAM while MT-3 cells (German Collection of Microorganisms and Cell Cultures, (Deutsche Sammlung von Mikroorganismen und Zellkulturen (DSMZ)), Braunschweig, Germany) express high levels of Ep-CAM, as published by Prang, et al, British Journal of Cancer, 2005.

Cells were maintained in Dulbecco's Modified Eagle Medium – Nutrient Mixtures F12 (DMEM/F12) with 10% fetal bovine serum (FBS) in a humidified incubator with 5% CO_2 at 37^{o}C. Cell culture reagents were purchased from Gibco/Invitrogen (Carlsbad, CA) and supplies, including sterile tubes, cell culture flasks and pipettes were purchased from ISCBioexpress (Kaysville, UT) or VWR (Radnor, PA). On the day of experimentation, cells were rinsed in phosphate buffered saline (PBS) and incubated in trypsin for 10-20 minutes. After cells were sufficiently detached from the cell culture flasks, they were removed from the flasks and spun down.

For cell binding, the cells were split into tubes each with one million cells, and washed in hanks based salt solution (HBSS) with bovine serum albumin (BSA). Each tube of one million cells was incubated with 1 ng of anti-Ep-CAM-IR800 for 30 minutes to one hour a humidified incubator with 5% CO_2 at 37^{o}C. Unbound antibody was washed off the cells with HBSS-BSA and antibody binding was determined using flow cytometry (FACSAria, BDBiosciences, San Jose, CA), microscopy (Lieca, Bannockburn, IL), or the Odyssey (Licor, Lincoln, NE). Cell nuclei were stained using Sytox Green (Invitrogen, Carlsbad, CA).

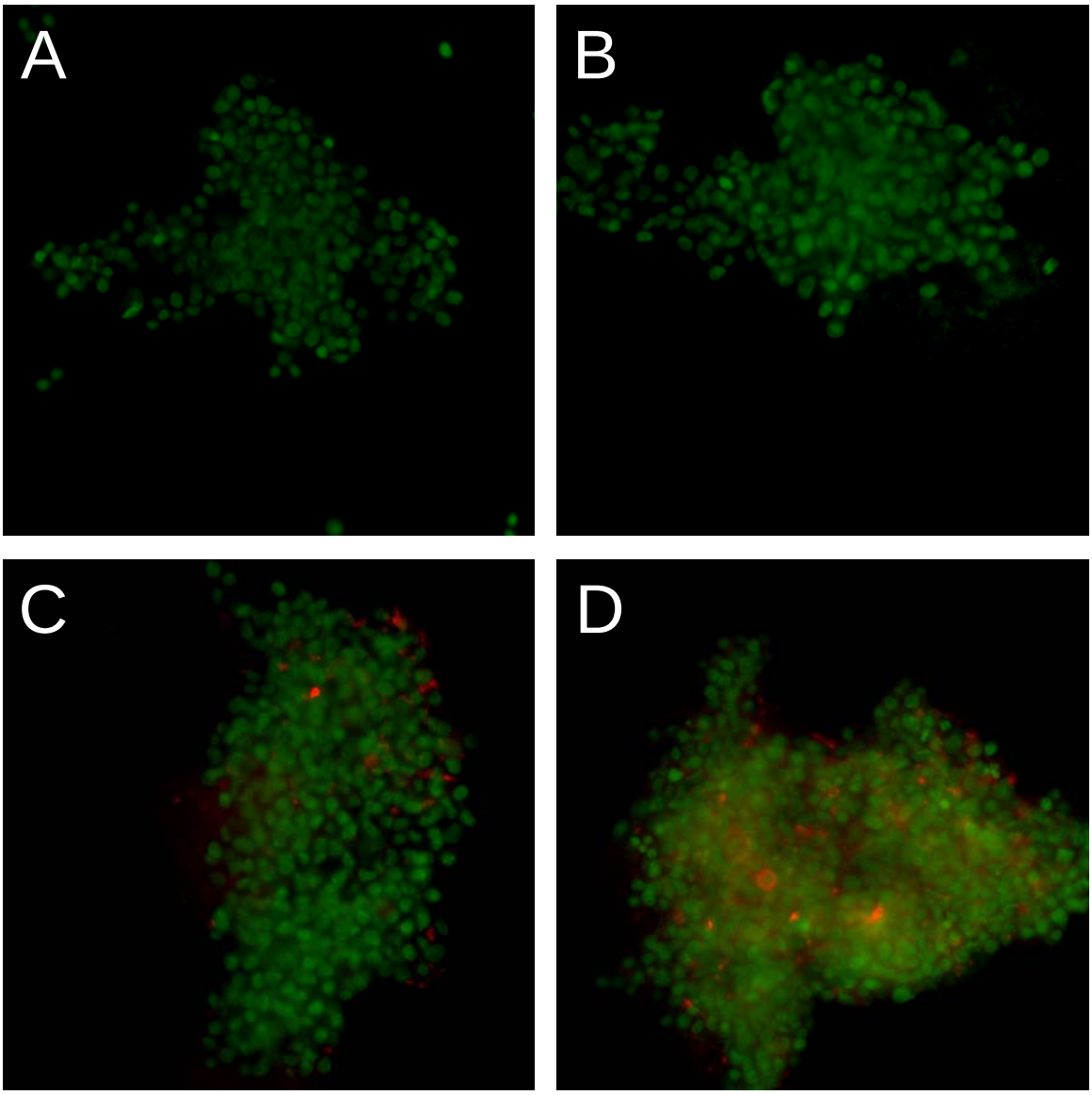

Figure 1: Two human breast cancer cell lines SKBr3 (A,C) and MT-3 (B,D) were stained with an anti-EpCAM antibody (red in C,D) and cell nuclei were stained with sytox green (green in all panels). More anti-EpCAM antibody binding is seen on the high Ep-CAM expressing MT-3 cells than on the low Ep-CAM expressing SKBr3 cells.

Stability and pH sensitivity of anti-Ep-CAM agent, moving towards dual-labeled in vivo imaging, the anti-Ep-CAM antibody mAb 9601 was labeled with IRDye, Alexafluor 680 or IRDye and Alexafluor 680 in different buffers at different pH levels to test the binding ability of the antibody after conjugations. Labeled antibodies were measured for dye to protein ratios and protein concentration, as described in Table 1.

Buffer	mAb9601-IRDye 800CW		mAb9601-AF680	
	D:P	[] mAb mg/ml	D:P	[] mAb mg/ml
Sodium Bicarbonate pH 7.4	2.4	0.12	2.5	0.13
Sodium Bicarbonate pH 8.0	1.2	0.28	1.5	0.20
Sodium Bicarbonate pH 8.2	2.5	0.17	2.3	0.26
Sodium Phosphate pH 8.3	2.7	0.26	0.62	0.05

Table 1: Comparison of conjugation efficiency of dye to antibodies in reaction buffers.

The samples were then incubated on breast cancer cells to determine their ability to bind to high Ep-CAM expressing cells (MCF-7 and MT-3) and low expressing cells (SKBr3). The images shown are from the Alexafluor 680 labeled antibody.

Unfortunately there was too much overlap between the AF680 and IRDye 800 absorbance measurements, so I was unable to quantify the amount of each dye that labeled the antibody in the dual conjugation. HPLC traces were run of each antibody conjugate to determine if there was free dye present after the purification processes and the traces did not show free dye contamination (data not shown).

The HPLC tubes were imaged on the Odyssey imager to determine if the fluorescent signal was sufficient for a cell binding assay as shown in figure 2.

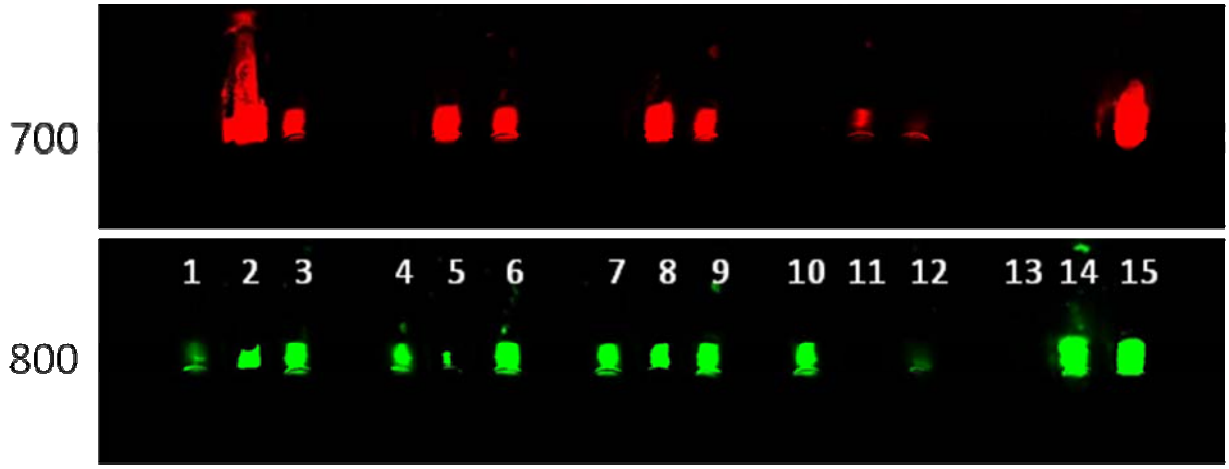

Figure 2: Fluorescent images of labeled antibodies for Alexafluor 680 (em 710 nm) and IRDye 800CW (em 830 nm).

The sample numbers from figure 2 are explained in detail in table 2. The first column is sample number, then buffer, pH, labeling ratio of IRDye to antibody and finally labeling ratio of Alexafluor 680 to antibody. The labeling ratios were controlled so that each antibody received a maximum of 5-fold excess dye to ensure retention of binding ability.

Sample	Buffer	pH	IRDye:Ab	AF680:Ab
1	$NaHCO_3$	7.4	5	0
2	$NaHCO_3$	7.4	0	5
3	$NaHCO_3$	7.4	2.5	2.5
4	$NaHCO_3$	8.0	5	0
5	$NaHCO_3$	8.0	0	5
6	$NaHCO_3$	8.0	2.5	2.5
7	$NaHCO_3$	8.2	5	0
8	$NaHCO_3$	8.2	0	5
9	$NaHCO_3$	8.2	2.5	2.5
10	Na_2HPO_4	8.3	5	0
11	Na_2HPO_4	8.3	0	5
12	Na_2HPO_4	8.3	2.5	2.5
13	10 mg Ab in 100 ml PBS	7.4		
14	5 mg IRDye in 100 ml PBS	7.4		
15	5 mg AF680 in 100 ml PBS	7.4		

Table 2: Summary of labeled antibody samples in different buffers, pHs and with differing amounts of IRDye and Alexafluor 680.

The fluorescent intensities of the different antibody conjugates were measured and the results summarized in figure 3.

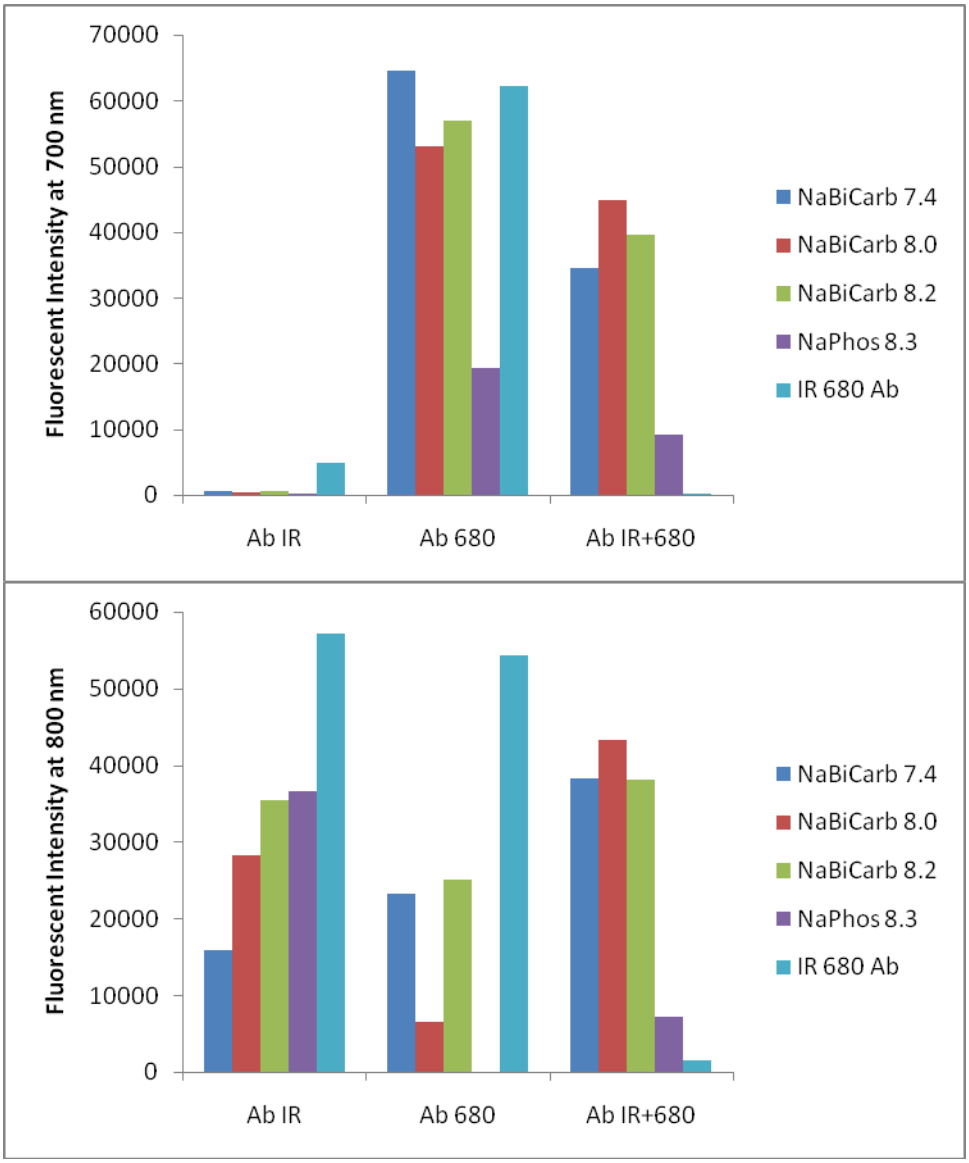

Figure 3: Fluorescent intensity of the labeled antibodies, with each bar of the final data set representing a control, the first bar is IRDye800 only, the second bar is AF680 only, and the third bar is unlabeled antibody only. There is a contribution at 800nm from the AF680, but no contribution at 700 from IRDye800.

In both charts the final data set is IRDye (sample 13), AF680 (sample 14), and antibody with no dye (sample 15). The antibody conjugates were then diluted in a phosphate buffered saline at pH 7.4 for cell binding studies. Three cell lines were used, MCF-7 and MT-3, high Ep-CAM expressing cells, and SKBr3, low Ep-CAM expressing cells. In previous experiments (data not shown) the binding of anti-Ep-CAM to the cells is very dependent upon the confluence of the cells at the time of harvest. The MT-3 and SKBr3 cells shown in figure 4 were grown to 100% confluence, the media changed, and then left to grow for another 3 days. The MCF-7 cells were grown to 70% confluence, the media changed, and then left to grow for another 3 days. In the binding results below, the high Ep-CAM cells that were grown well past confluence displayed the most binding. This is probably explained by the fact that Ep-CAM is an adhesion molecule, so in the presence of more cells for binding interactions, each cell might produce or display more Ep-CAM for binding.

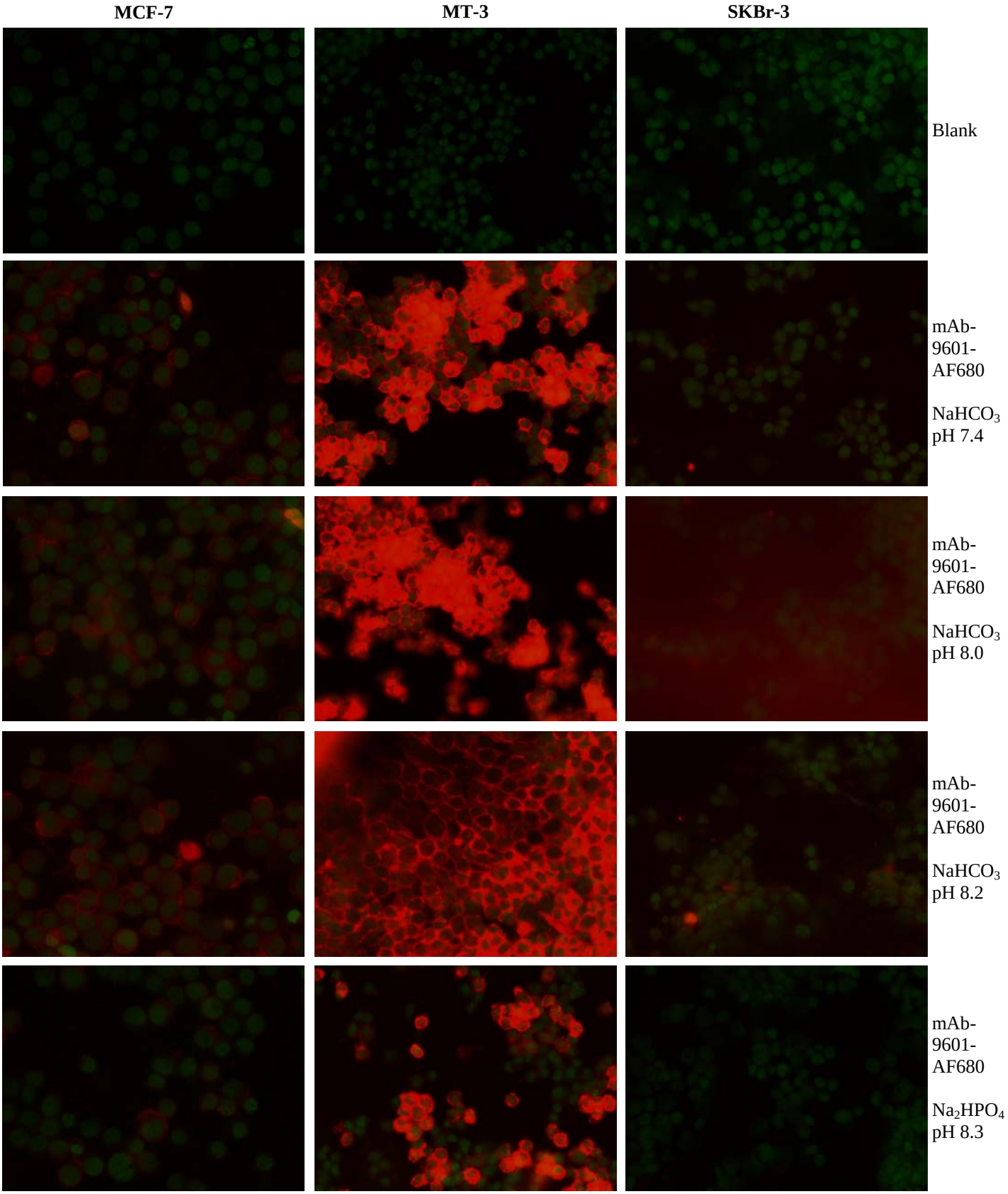

Figure 4: Binding of labeled anti-Ep-CAM antibody (9601) to high Ep-CAM expressing MCF-7 and MT-3 cells and low Ep-CAM expressing SKBr3 cells.

The antibody conjugates retained their ability to bind Ep-CAM positive breast cancer cells in pH up to 8.3, which will be important for the chelating agent DOTA. The DOTA-NHS-ester is best conjugated between pH

8.0 and 8.5, so the ability of the antibody conjugate and dyes to withstand a pH above 8 will allow the dual-labeling of anti-Ep-CAM for animal studies.

For dual-labeled in vivo imaging, the antibody must be conjugated with the fluorophore (IRDye 800CW) and a chelating agent (DOTA), which sequesters the radio-metal completing the dual-label. Each conjugation step requires an incubation of 4 hours to overnight, so to determine the best order of conjugation or if the conjugations could be done simultaneously, anti-Ep-CAM (9601) was conjugated with 5-fold excess IRDye, 5-fold excess DOTA or 500-fold excess DOTA overnight. After size exclusion and centrifugation to remove non-conjugated IRDye or DOTA, the 9601-IR samples were conjugated with 5- or 500-fold excess DOTA, the 9601-DOTA samples were conjugated with IRDye, and a fresh batch of 9601 was conjugated with 5-fold excess IRDye and DOTA (at either 5- or 500-fold excess) overnight at 4 degrees. Two samples of 9601 were kept unlabeled for testing purposes, one was unprocessed and the other went through all processing steps but without any dye or DOTA for conjugation.

Sample	Conjugation 1	Purification 1	Conjugation 2	Purification 2
9601-unp	NO	NO	NO	NO
9601-p	Buffer	YES	Buffer	YES
9601-IR,D	5xIRDye	YES	5xDOTA	YES
9601-D,IR	5xDOTA	YES	5xIR	YES
9601-D5,IR	500xDOTA	YES	5xIR	YES
9601-IR-D	Buffer	YES	5xIR+5xDOTA	YES
9601-IR-D5	Buffer	YES	5xIR+500xDOTA	YES
IT-IR-D	Buffer	YES	5xIR+5xDOTA	YES

Table 3: Conjugation ratios and conditions for anti-Ep-CAM (9601), IRDye 800CW (IR), and the chelating agent, DOTA.

The ability of these different conjugates to bind to Ep-CAM positive cells was then tested using flow cytometry. Ep-CAM positive MT-3 cells were grown to confluence, trypsinized, washed and $1x10^6$ cells were placed into tubes for antibody binding. The different conjugates and controls of IRDye in DMSO, IRDye in PBS, and buffer with no agent were incubated with cells for 1 hour at 37 degrees. After 1 hour the cells were washed to remove unbound antibody and then secondary antibody, goat anti-mouse-Alexafluor488 (GaM-488) was incubated with the cells to detect presence of mouse antibody. The flow cytometer measuredAlexafluor488 (figure 5) and IRDye 800CW (figure 6) fluorescence in each sample through mean fluorescent intensity and percent positive.

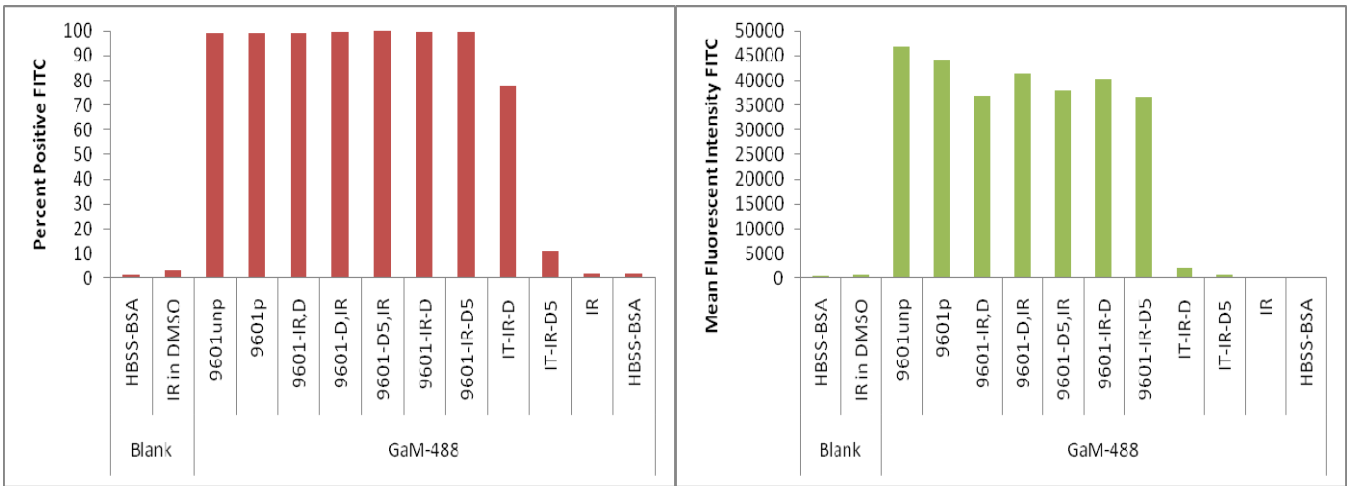

Figure 5: Binding of dual labeled anti-Ep-CAM-IR800-DOTA to Ep-CAM positive MT-3 cells measured using percent positive and mean fluorescent intensity of goat anti-mouse Alexafluor 488 secondary antibody.

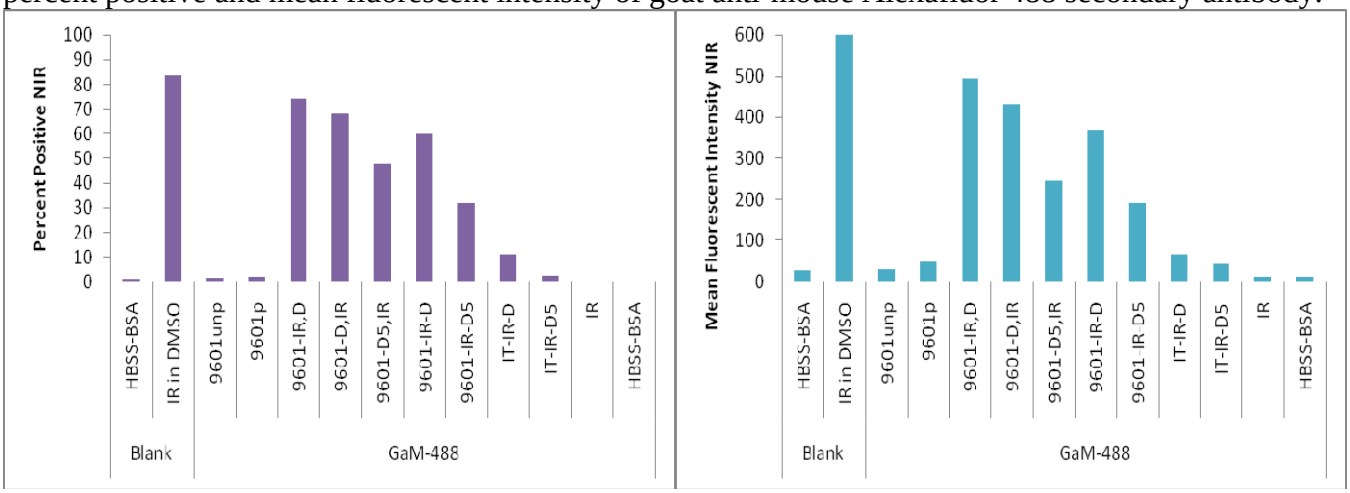

Figure 6: Binding of dual labeled anti-Ep-CAM-IR800-DOTA (9601-IR-D) to Ep-CAM positive MT-3 cells directly measured using the IR800 fluorescence from the labeled antibodies.

In addition to using flow cytometry to measure the fluorescent intensity, the NIR binding of these antibody conjugates was determined using the Odyssey (Licor, Lincoln, NE) to scan for IR800. Ep-CAM positive, MT-3 cells, and low Ep-CAM expressing, SKBr-3 cells were placed in a 96-well dish and allowed to grow to overconfluence, then washed and incubated with anti-Ep-CAM antibody for 1 hour at 37 degrees, then washed and incubated with secondary antibody, goat anti-mouse-Alexafluor-488 for 1 hour at 37 degrees. After a final wash, the plates were imaged on the Odyssey. The SKBr3 cells used in this experiment were previously transfected with the gene for near infrared protein 1.4 (IFP1.4) so by scanning for both IFP and IRDye, the relative number of cells in each well can be determined in addition to the amount of antibody binding. The scales are very different in the two graphs, with very little binding detected in the SKBr3 cells. The IFP levels detected were also very low, this is probably because biliverdin, which enhances IFP signal, was not added to the cells to ensure any 800nm signal detected was due to the IRDye as seen in figure 7

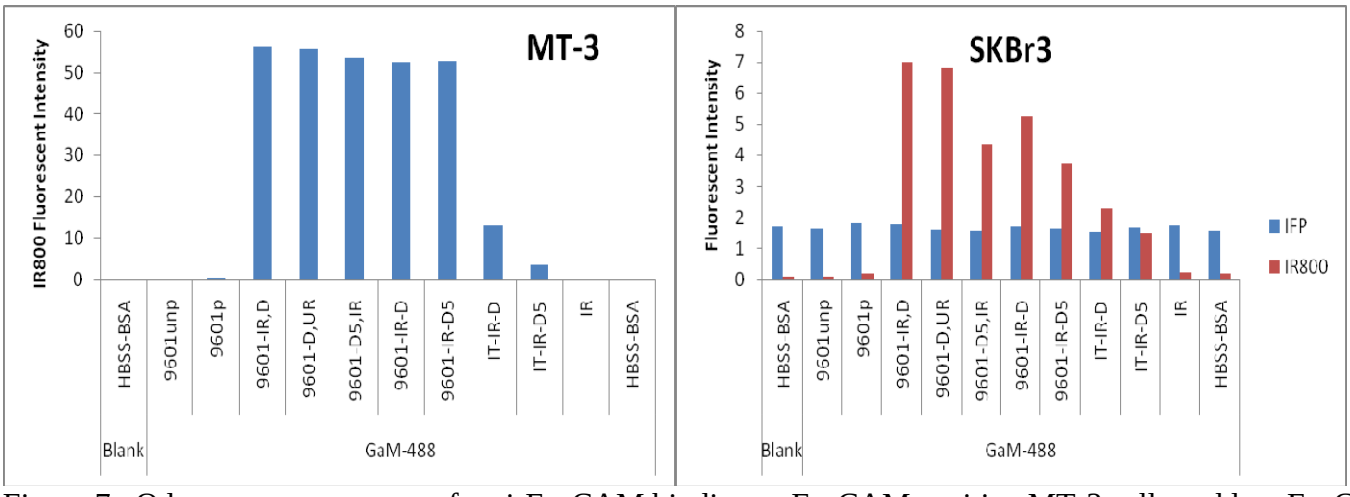

Figure 7: Odyssey measurement of anti-Ep-CAM binding to Ep-CAM positive MT-3 cells and low Ep-CAM expressing SKBr3 cells. The IFP measured in the SKBr3 cells shows that each well had a similar amount of cells present.

From the cell binding experiments, it was determined that labeling the antibody with IRDye first and then the chelating agent, at a 5-fold excess, produces the conjugated antibody with the best binding to Ep-CAM positive cells.

In addition to DOTA, another chelating agent, NOTA, which has an NCS functional group, and requires a higher pH for conjugation, was explored due to its ability to chelate both Copper and Gallium. It was determined that a pH of 9 or greater was the best of chelating NOTA and that the antibody retained the ability to bind to Ep-CAM positive cells.

MCF-7 cells, which express high levels of Ep-CAM were grown in a 12 well dish and incubated with isotype (IT) or anti-Ep-CAM (9601) at 37 degrees to determine the cell binding properties of the antibody conjugates produced under different conjugation conditions. It was determined that 10 or 20 fold excess of NOTA and pH 9.0 did not appreciably decrease the cell binding ability of the antibody, shown in figure 8.

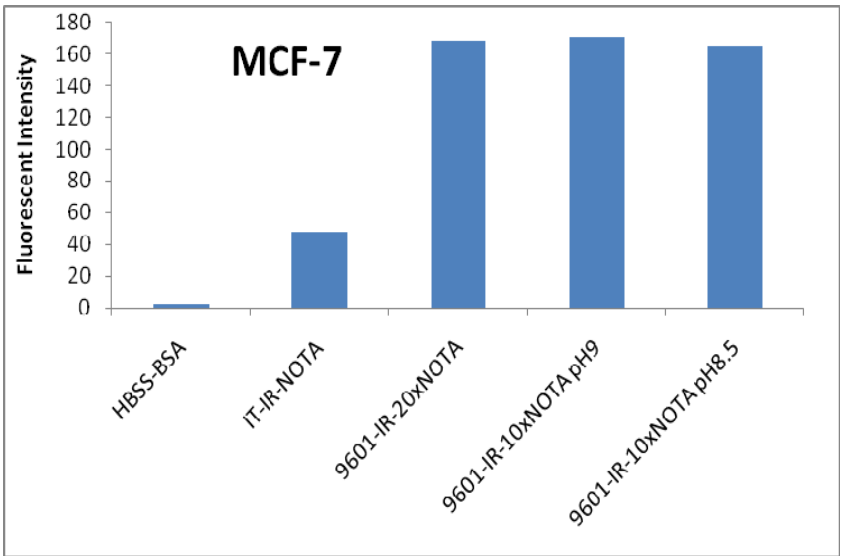

Figure 8: Odyssey measurement of anti-Ep-CAM-IR-NOTA binding to Ep-CAM positive MCF-7 cells. The conjugation of NOTA at 10 and 20-fold excess did not appreciably reduce the cell binding, nor did the use of mildly basic pH conditions.

After confirming retention of binding ability in the NOTA and IRDye labeled antibody, the next step was to determine the reaction conditions for the chelation of Ga-67. One main reason for the use of NOTA as a chelating agent is that the chelation step only requires 15 minutes at room temperature and the quenching of free Ga-67 with an unbound chelating agent (EDTA) is an additional 15 minutes making the full preparation approximately an hour including the chelating measurement. After each chelation step a 1 ul sample is measured using thin layer chromatography to determine the percent chelation of the radio-metal.

The dual-labeled antibodies were then tested for cell binding ability as well as retention of IR800 signal and Ga-67 radioactivity. The Ep-CAM overexpressing MT-3 cells were incubated with different formulations of dual-labeled IT and 9601. The 9601 retained ability to bind to Ep-CAM positive cells as shown in figure 9 with both IR800 fluorescent signal and radioactive counts.

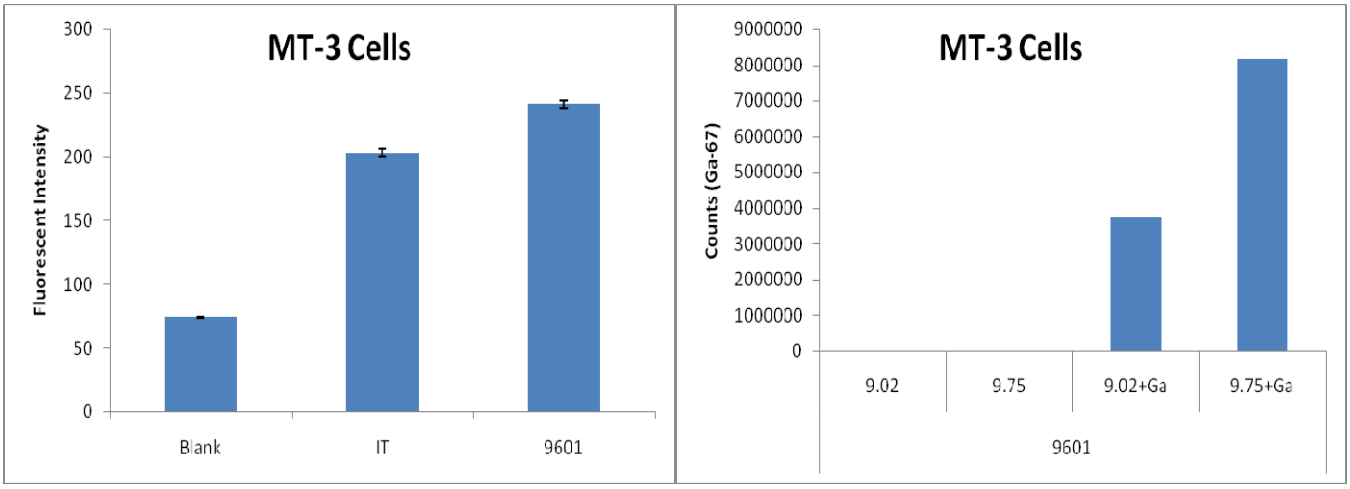

Figure 9: Cell binding of anti-Ep-CAM (9601) and isotype (IT) antibodies after chelation of Ga-67. The graph on the right shows that the IR800 signal is retained after the chelation and the graph on the right compares the relative chelation ability of 9601 labeled with NOTA at pH 9.01 and pH 9.75. The NOTA conjugation is more efficient at higher pH allowing for chelation of more Ga-67.

The anti-Ep-CAM antibody, 9601-IR800-NOTA-Ga-67, was formulated and retained cell binding and NIR signal after the chelation of Ga-67 giving an active, fluorescent, radioactive binding agent for detection of Ep-CAM positive cancer. This agent was then tested in nude mice with xenograft tumors of human breast cancer cells MCF-7 and MT-3 in the right flank.

Phase I of the preclinical anti-Ep-CAM imaging which included: binding affinity studies, antibody labeling, HPLC validation, stability studies, testing of the affinity of dual-labeled antibody, and specificity (blocking) assays was completed, resulting in the generation of a dual-labeled anti-Ep-CAM antibody (9601-IR-NOTA-Ga-67) which bound specifically to Ep-CAM positive breast cancer cells.

Phase II of the preclinical anti-Ep-CAM imaging included generating breast cancer tumors in the lymph nodes of mice, determining the antibody clearance rates, and determining the WBC clearance of antibodies.

Cancer, other diseases, or infections can cause lymph nodes to become swollen and reactive. This can be part of a whole body or localized immune response. Before determining that our agent is specifically binding to cancer cells, we must first determine that the antibody is not retained more significantly in swollen, reactive nodes than in other nodes.

Balb/C mice were injected in the dorsal aspect of the left forepaw with a bacterial wall polysaccharide (LPS) to cause a local immune response. A few days later, the mice were injected in the dorsal aspect of both forepaws with an anti-EpCAM antibody labeled with a NIR dye. Images were taken of the left and right sides of the mice to detect the amount of antibody in each node. Figure 10 displays the images from 6, 24, and 48 hours post anti-Ep-CAM administration.

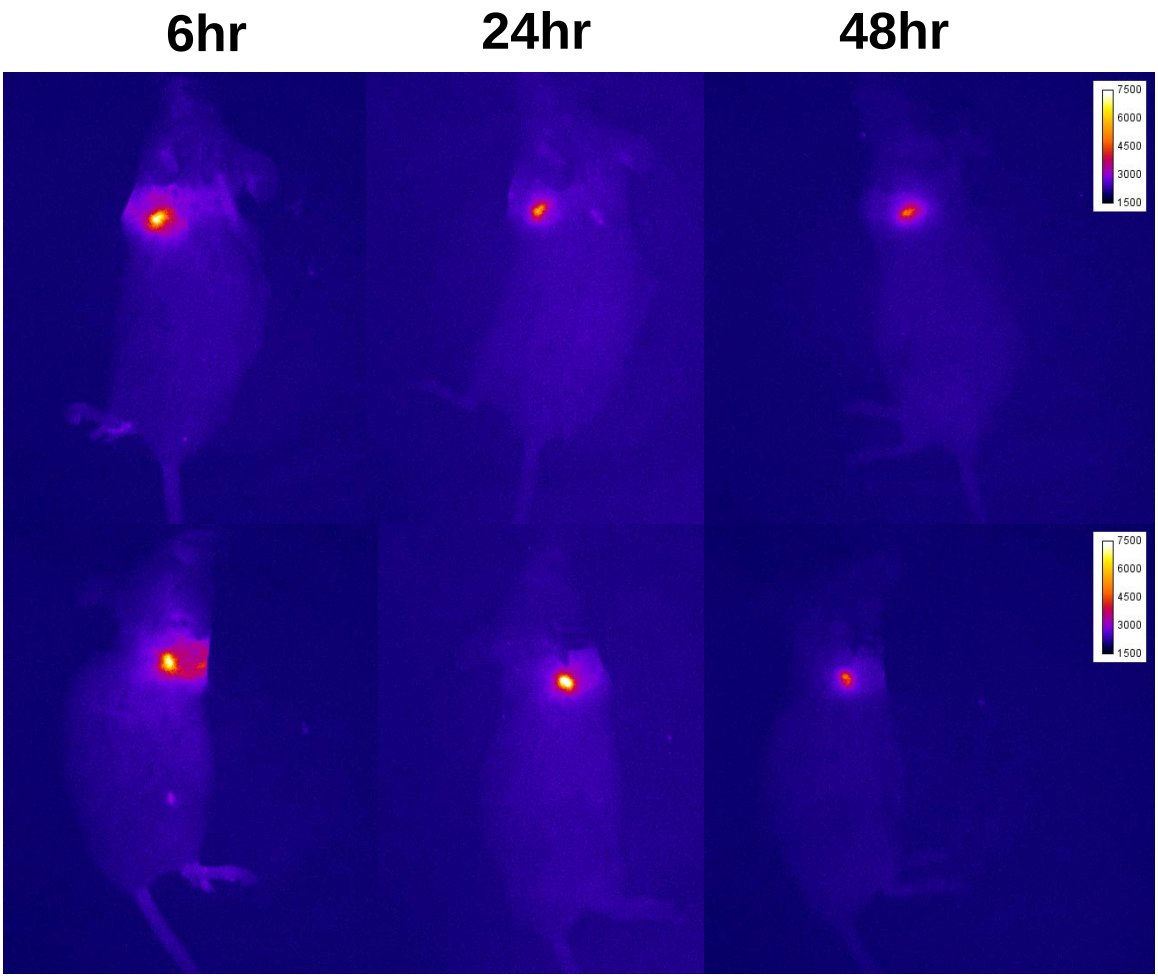

Figure 10: Pseudo color images of BALB/C mice viewing the left (top row) or right (bottom row) side of the mouse at different time points after the injection of the anti-Ep-CAM-IR800. The left paw received an injection of LPS to illicit an immune response a few days before the antibody injection. The images show similar levels of fluorescence in the left, immune reactive lymph node and in the contra lateral control, right lymph node.

Visually, the right and left lymph nodes appear similar (figure 11), so regions of interest were defined around the left and right lymph nodes at each time point to calculate the exact fluorescent signal from the lymph nodes. The NIR signals from the right and left axillary lymph nodes were averaged for the 5 mice at the different time points and graphed in figure 3. Using this method, we determined the clearance rate of antibodies from the normal (right) and immune reactive (left) lymph nodes.

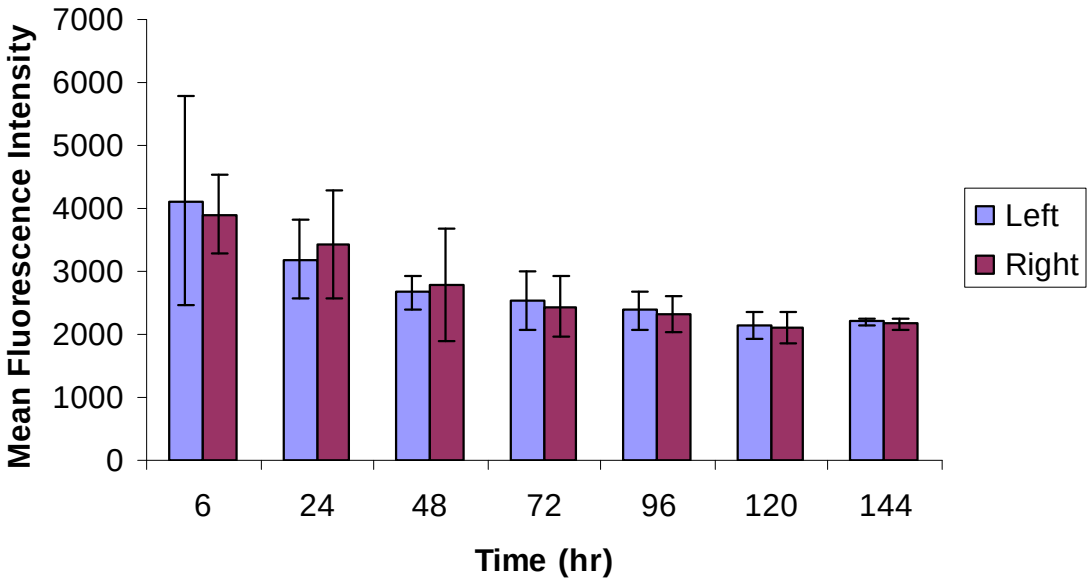

Figure 11: Mean fluorescent intensity of the axillary lymph nodes of BALB/C mice. The immune reactive (left) and contra lateral, control (right) axillary lymph nodes cleared the anti-Ep-CAM-IR800 antibody at about the same rate. At the early time points, a large range of NIR signals was seen in the lymph nodes of the mice.

This graph shows that while there is variability at the earliest time point, there is no statistical difference between antibody retention in the swollen, reactive lymph nodes (left) and the contra lateral, normal control lymph nodes (right). Therefore, if higher antibody levels in cancer positive lymph nodes, can be attributed to the presence of cancer, rather than an immune response.

Tumor generation has been achieved by directly injecting cells into the lymph nodes of mice delivering a known number of the cells to the lymph node, but damages the lymph node severely. Injection of tumor cells into the mammary fat pads, and allowing the tumor cells migrate to the lymph nodes is a better model of metastasis, but introduces variability in the number of cells that reach the lymph nodes and the timeline for reaching the lymph nodes. Figure 12 displays a diagram of the murine mammary fat pads and the general locations for these two tumor inoculation methods.

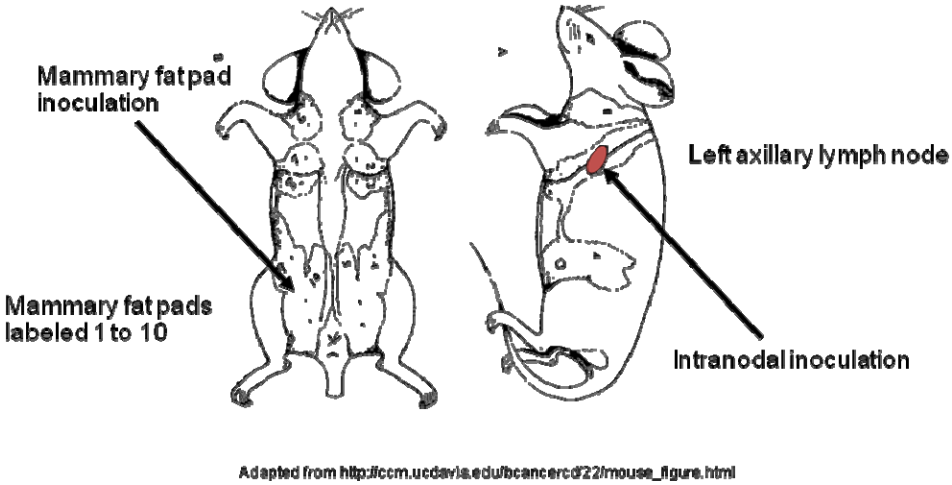

Figure 12: Schematic representation of murine mammary fat pads with arrows highlighting injection sites for breast cancer tumor cell inoculations.

Previously the tumors were allowed to form until just palpable and then the anti-Ep-CAM agent was delivered. To detect micro-metastases, the agent must be delivered before the tumor is palpable. The following work with IFP1.4 was not initially proposed in the grant application, the original work discussed the use of dsRed or mCherry stable cells. When a new fluorescent protein in the far red/near infrared region was discovered by Dr. Tsien's laboratory in San Diego, we contacted him to learn about the infrared protein, IFP1.4, which could be expressed in human cells.[8-9] Dr. Tsien kindly sent a sample which was cloned into a lentivirus and an adenovirus for transfection of breast cancer cells. The transfected cells were sorted for a population expressing high levels of IFP1.4 using fluorescence activated cell sorting. The cells were imaged for IFP1.4 fluorescence (ex 680, em 700) using the Odyssey Imager (Licor Biosciences, Lincoln, NE), shown in Figure 13. The IFP1.4 fluorescence is not visible in the IRDye 800CW range (ex 785, em 830, data not shown), so it will not interfere with agent detection.

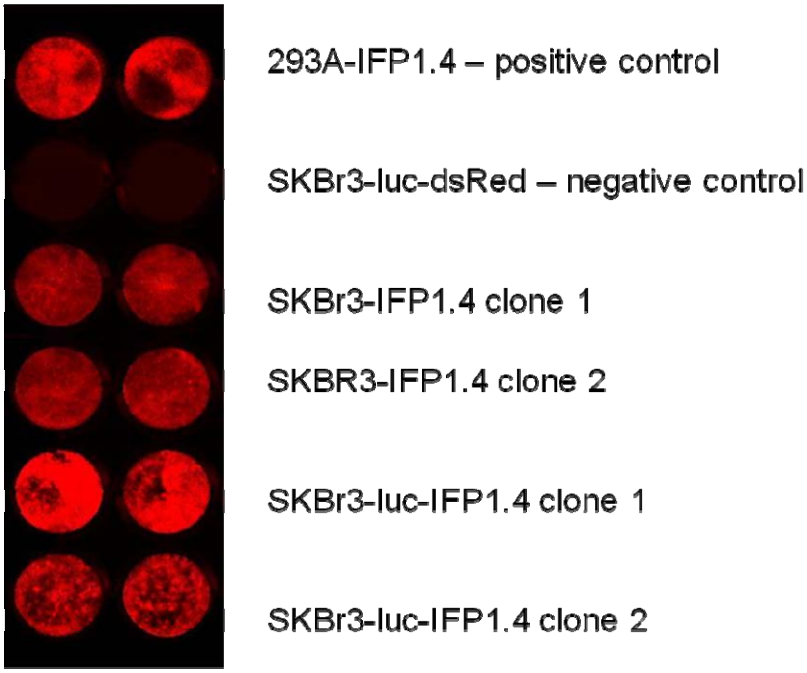

Figure 13: Pseudocolor image of human breast cancer cells expressing the infrared fluorescent protein IFP1.4.

The development of intranodal tumors and the metastatic spread of mammary fat pad tumors will be monitored using the IFP1.4 fluorescent tumors. Monitoring the mammary fat pad tumors will help me to learn the grown kinetics of the primary tumor and the metastasis timeline; this will enable earlier delivery of agent, hopefully leading to earlier detection of metastatic cells.

The highly sensitive imaging of fluorescent emitted light requires specific imaging devices be built for each different fluorophore. IFP1.4 has an excitation maximum of 684nm and an emission maximum of 708nm. We were able to use the same EMCCD (electron multiplying charge coupled device) camera from Princeton Instruments (Trenton, NJ) because it has high sensitivity to signals between 400 and 900nm. The imaging system used for NIR fluorescent imaging was modified for far red imaging for imaging of the IFP stable cells. A 668nm excitation laser was mounted to the camera and a diffuser and laser line clean up filter placed in front of the diode. Holographic and bandpass filters were placed in front of the CCD camera to collect the 690 emission light. The imaging system is shown in Figure 14.

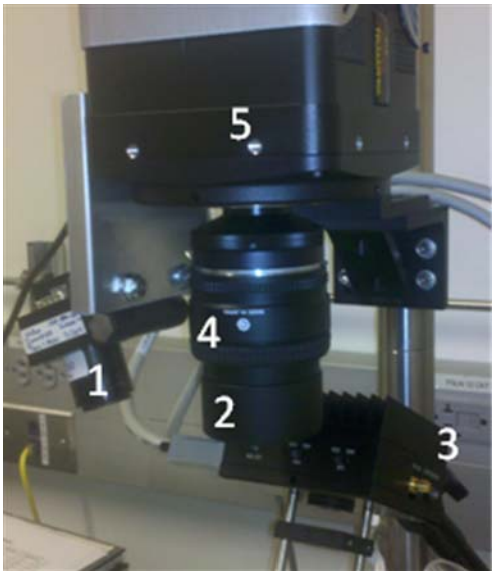

Figure 14: Imaging system: Fluorescent dyes are excited using a laser (1) 668nm far red or (3) 785nm NIR and the resulting emitted fluorescent light goes is collected after passing through bandpass and holographic filters (2). The filters collect 690nm and 830nm emitted light, for far red and NIR fluorophores respectively. After passing through the filter sets the light is focused through a lens (4), collected by the CCD camera (5), and saved to a computer (not shown).

After setting up the new wavelength imaging capabilities, I tested the ability of the camera to image breast cancer cells stably expressing IFP1.4. Cells were cultured in DMEM/F12 with 10% FBS at 37^{o}C with 5% CO_2 in a humidified environment. Cells were incubated with biliverdin (25μM) for 24 hours then trypsinized and resuspended in plain DMEM/F12 and imaged for 500ms, as seen in figure 15.

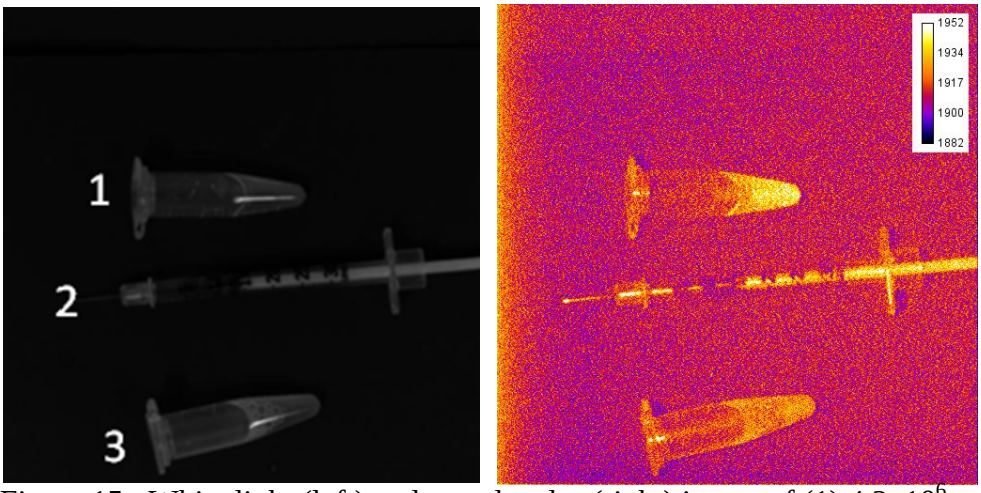

Figure 15: White light (left) and pseudocolor (right) image of (1) 4.2x10^{6} SKBr3-Luc-IFP1.4 cells in 400μl DMEM/F12, (2) 100μl DMEM/F12 in a 300μl insulin syringe, and (3) 4.2x10^{6} SKBr3-IFP1.4 cells in 400μl DMEM/F12.

The IFP stable cells were inoculated into the mammary fat pad or subcutaneously on the dorsal side of the mouse. Images were taken of each mouse just after injection, and then weekly to determine the growth kinetics of the tumor cells. Figure 16 shows one mouse from each group on the day of inoculation (Day 0).

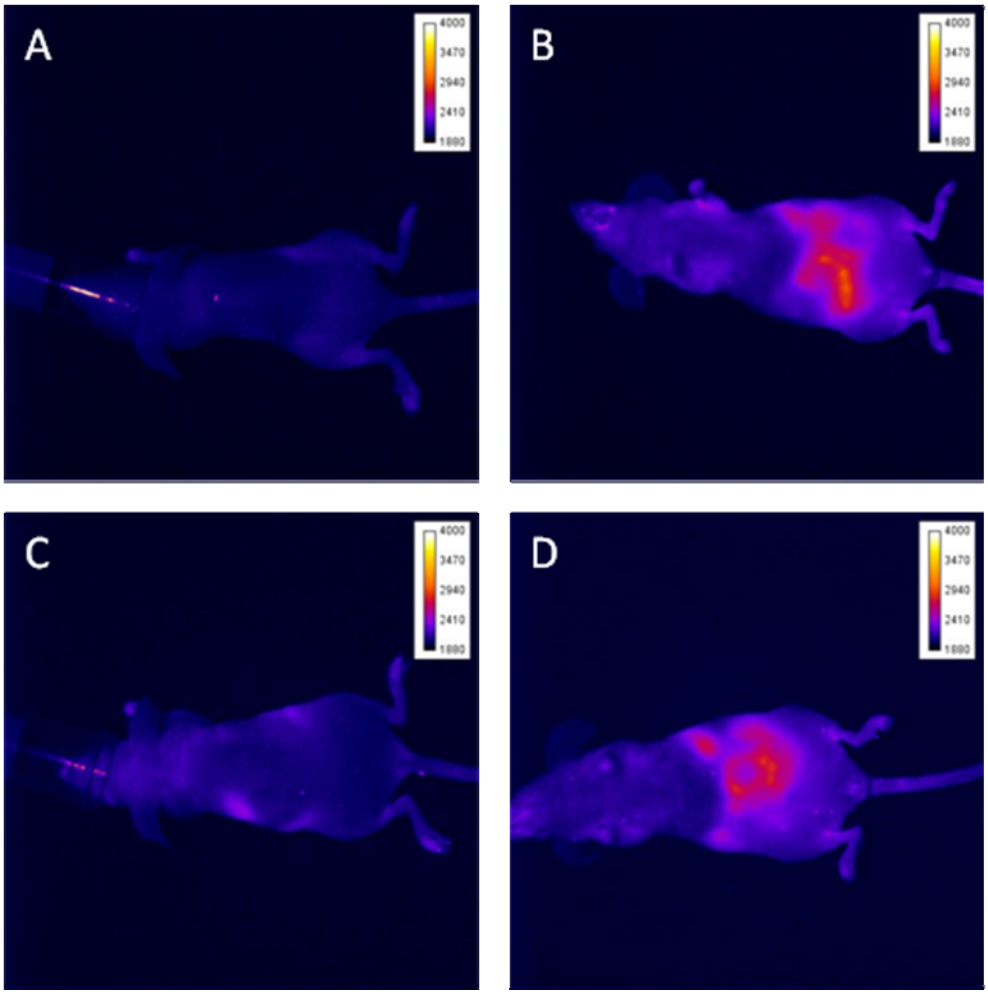

Figure 16: Pseudocolor images of nude mice after inoculation of tumor cells, SKBr3-Luc-IFP1.4 subcutaneously in the left flank (A) or in the 7th mammary fat pad (B) and SKBr3-IFP1.4 subcutaneously in the left flank (C) or in the 7th mammary fat pad (D). Each mouse shown here received an injection of 100,000 cells in 100µl and a control injection of 100µl DMEM/F12 on the contralateral side.

Unfortunately with the far red imaging, there is a large amount of background signal due to the chlorophyll in the food the mice eat. The intestines are clearly delineated, with loops sometimes visible. In the initial images there was a lot of excitation light leakage. To combat this issue, I added a laser clean up filter in front of the laser, which significantly reduced the amount of excitation light leakage. Mice are imaged every week to track the tumor growth; the images in Figure 17 were taken 19 days after inoculation of tumor cells.

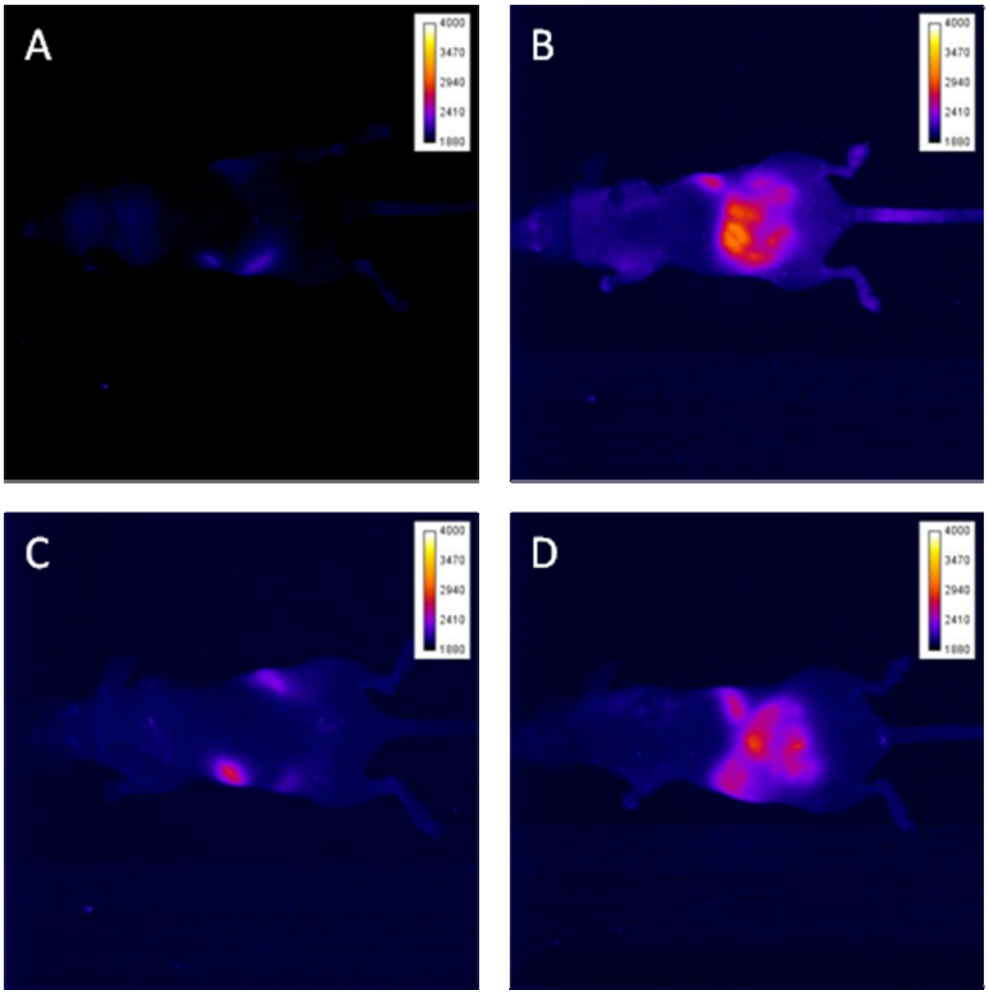

Figure 17: Pseudocolor images of nude mice 19 days after inoculation of tumor cells, SKBr3-Luc-IFP1.4 subcutaneously in the left flank (A) or in the 7th mammary fat pad (B) and SKBr3-IFP1.4 subcutaneously in the left flank (C) or in the 7th mammary fat pad (D). Each mouse shown here received an injection of 100,000 cells in 100µl and a control injection of 100µl DMEM/F12 on the contralateral side.

At day 25, one of the mice in the SKBr3-Luc-IFP1.4 subcutaneous group had a just palpable tumor which did not show up on the imaging (images not shown). This experiment in ongoing, so at the next imaging time point I should see IFP fluorescence at the tumor location.

Phase II of the preclinical anti-Ep-CAM imaging was completed. Although direct inoculation of breast cancer cells into the lymph nodes of mice did not always result in tumor formation (details to follow), I was able to generate tumors by inoculation the breast cancer cells subcutaneously into the flanks of the mice. Unfortunately the IFP1.4 tracking of the tumors was not as successful as hoped. This could probably be remedied by changing the diet of the mice. The high fluorescent signal from the intestines of the mice is actually from the chlorophyll in the feed, using a feed without chlorophyll would decrease the background signal, increasing my ability to image IFP1.4.

Phase III of the preclinical anti-Ep-CAM imaging involved generation of breast cancer tumors in the lymph nodes of mice, measuring antibody binding to tumors in the lymph nodes, blocking studies, histology, pathology, immunohistochemistry and biodistribution studies.

The human breast cancer cell line, SKBr3, was inoculated into the left axillary lymph node of nude mice and allowed to develop into tumors. When tumor nodules were just palpable, the mice were injected intradermally

with NIR-labeled anti-EpCAM and imaged at 6hr, 24hr, and 8 days. The 24 hour imaging time point is shown below in figure 18.

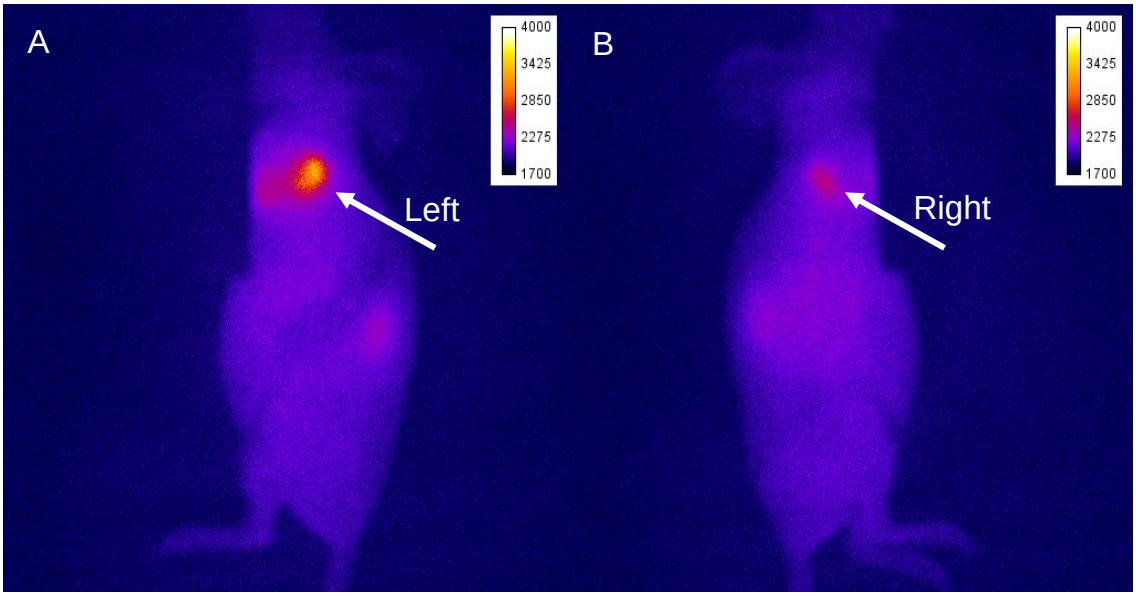

Figure 18: Psuedocolor image of left (A) and right (B) sides of a mouse with the axillary node locations indicated with arrows. The left axillary lymph node appears swollen and more fluorescent than the right.

The mice were imaged again at 8 days. Again, by defining regions of interest at the left and right axillary lymph nodes, the NIR signal was quantified to compare relative amounts of anti-EpCAM antibody, graphed in figure 19.

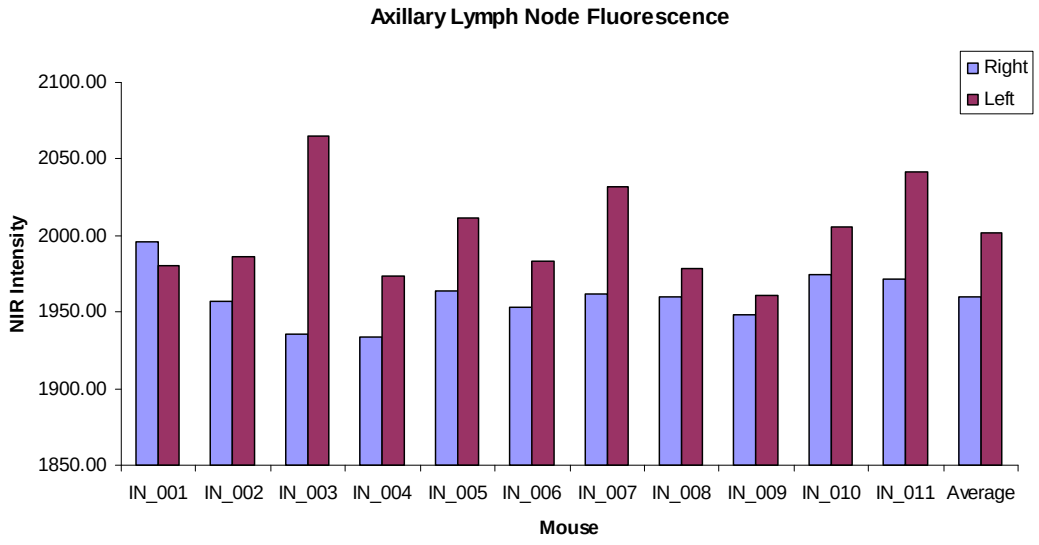

Figure 19: NIR fluorescent signal from the right (tumor negative) and left (possibly tumor positive) lymph nodes of nude mice eight days after intradermal injection of anti-Ep-CAM-IR800. There is a statistically significant difference ($p<0.005$) between the average of the right (tumor negative) and left (tumor positive) lymph node fluorescence.

On average the left (tumor bearing) axillary lymph nodes have higher fluorescent intensity, but by 8 days out, the amount of fluorescence had decreased significantly, but there was still a significant difference ($p<0.005$) in

the average of the right (tumor negative) and left (tumor positive) lymph nodes. After the whole body imaging, the mice were sacrificed and the organs imaged *ex vivo* to validate the whole body imaging. The excised organ images are shown below in figure 20.

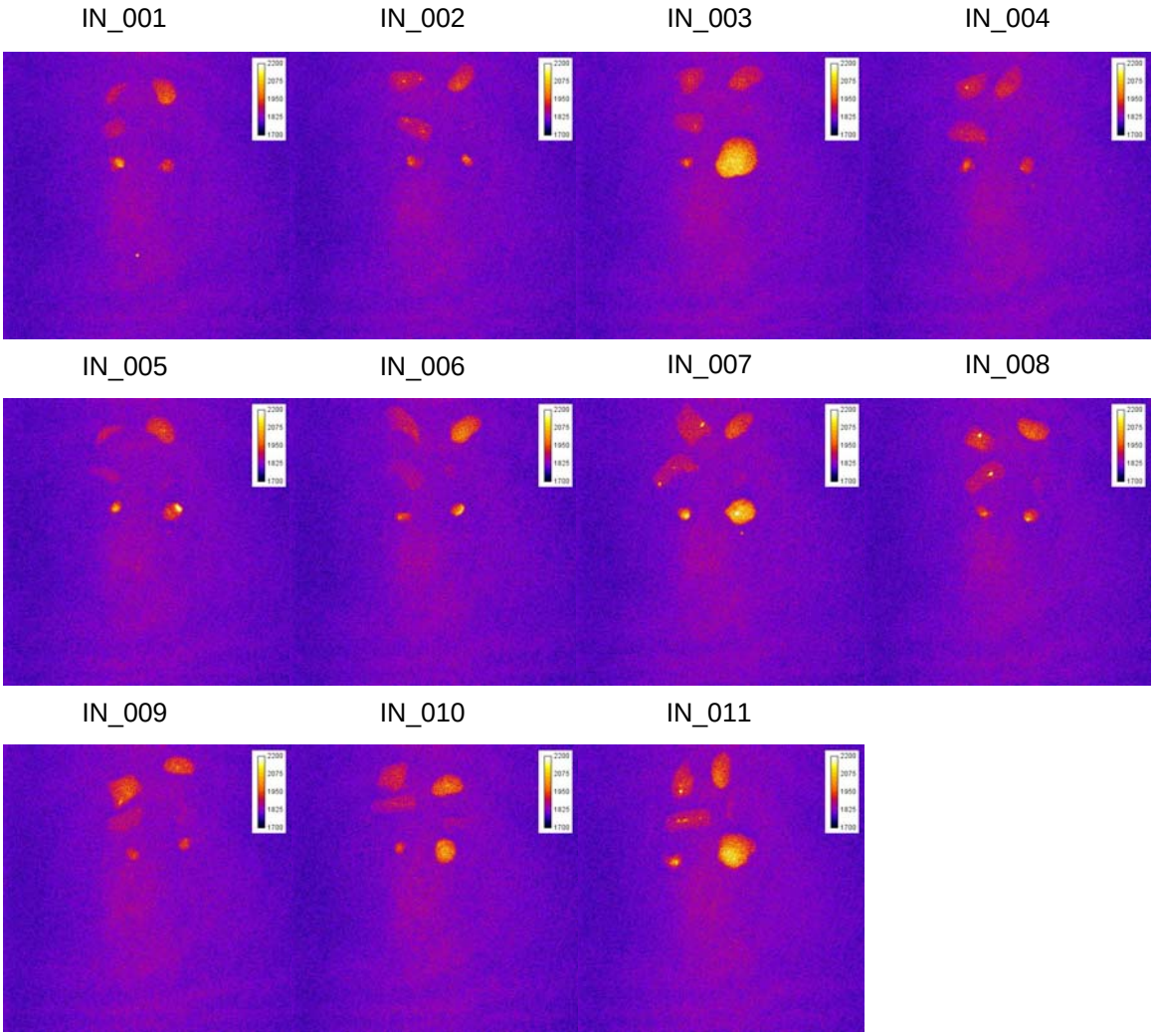

Figure 20: Pseudocolor image of excised organs, liver (top left), kidney (top right), spleen (middle left), muscle (middle right), right axillary node (bottom left), and left axillary node (bottom right). These images show very little background fluorescence in the liver, kidney, spleen and muscle, and that the left lymph nodes were enlarged and very fluorescent in mice IN_003, 007, 010, and 011.

The results from the whole animal and excised organ imaging indicated that the anti-Ep-CAM imaging agent bound specifically to breast cancer cells in the lymph nodes. Afterward, the organs were then frozen for H&E staining and immunohistochemical staining. The excised organ and histology images for one mouse (the same mouse shown in the whole body images in figure 18, IN_007) are shown in figure 21. The results show a higher NIR signal in the left axillary lymph node as compared with the right and the presence of SKBr3 cells in the left axillary lymph node and not the right, as shown by Her-2 expression on the SKBr3 cells.

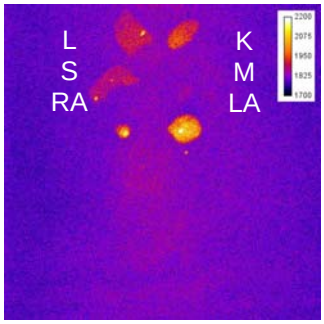

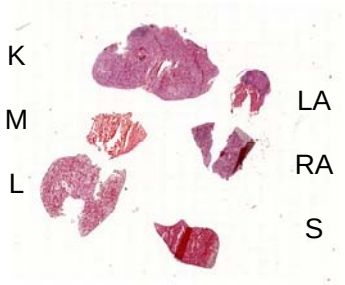

L – Liver
K – Kidney
S – Spleen
M – Muscle
RA – Right Axillary Lymph Node (tumor negative)
LA – Left Axillary Lymph Node (tumor positive)

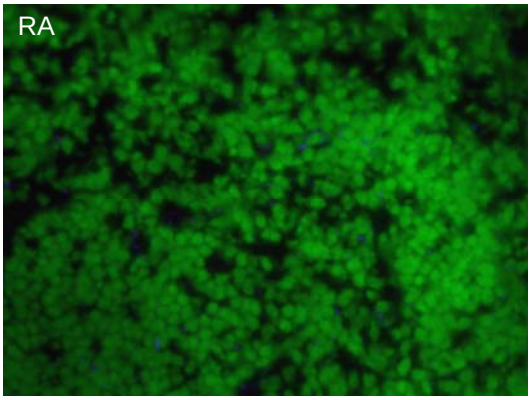

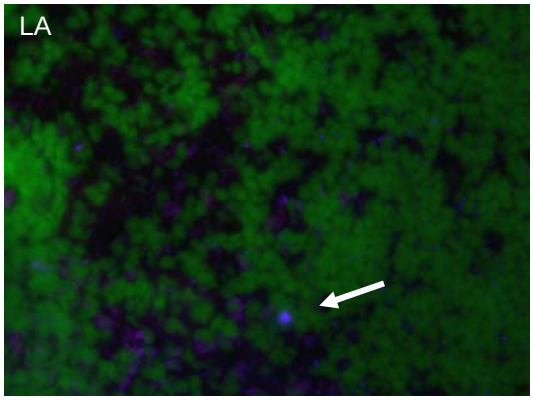

Figure 21: Pseudo color image of excised organs (top left), H&E staining of excised tissues (top right), and immunohistochemical staining of right (on left) and left (on right) axillary lymph nodes, show stronger NIR signal in the left axillary node than the right and the arrow in the bottom right panel shows presence of tumor cells in the left axillary lymph node.

The upper left panel shows the excised organ fluorescence, where the left axillary node is larger and has a higher IRDye 800CW signal indicating presence of anti-EpCAM-IRDye 800CW. The upper right panel shows the H&E staining of the excised tissues. The lower left panel displays 40x fluorescent images of the axillary lymph nodes stained with a nuclear stain, Sytoxin green (green), anti-Her-2 (red) and anti-EGFR (blue), the purple color indicates both Her-2 and EGFR presence. Presence of SKBr3 cells in the left axillary nodes is indicated by anti-EpCAM-IRDye 800CW, anti-Her2, and anti-EGFR.

The low amount of fluorescence seen in the tissue staining in figure 21 was consistent with the staining seen in the rest of the tissues. To try to better determine where the tumor formation was occurring, I brought the samples to the veterinary pathologist at Baylor College of Medicine. He reviewed the slides from 5 of the mice and said that he was unable to determine the presence of tumor nodules in the lymph nodes. This experiment was repeated with intranodal inoculation 2 times with the assistance of a veterinary technician, and the breast cancer tumors did not grow well in the lymph nodes of mice. Thus, for the purposes of testing the imaging agent, subcutaneous tumors were developed in the flanks of mice.

Human breast cancer tumor cells (MT-3) were inocculated subcutaneously in the right flank of nude mice with matrigel and allowed to form tumors for two weeks. Mice then received intravenously 200uCi doses of 9601-IR800-NOTA-Ga-67 and imaged at 4, 24, and 48 hours post injection. At the 24 hour time point the mice were euthanized and organs collected for further analysis.

SPECT images of the Ga-67 were taken using a DigiRad imager and each image represents a 5 minute acquisition time. The tumor is clearly visible in the mice who received the 9601 injections (highlighted by a white circles in figure 22) and the mice who received the free Ga injections. It is not present in the groups receiving the IT and NOTA-Ga injections.

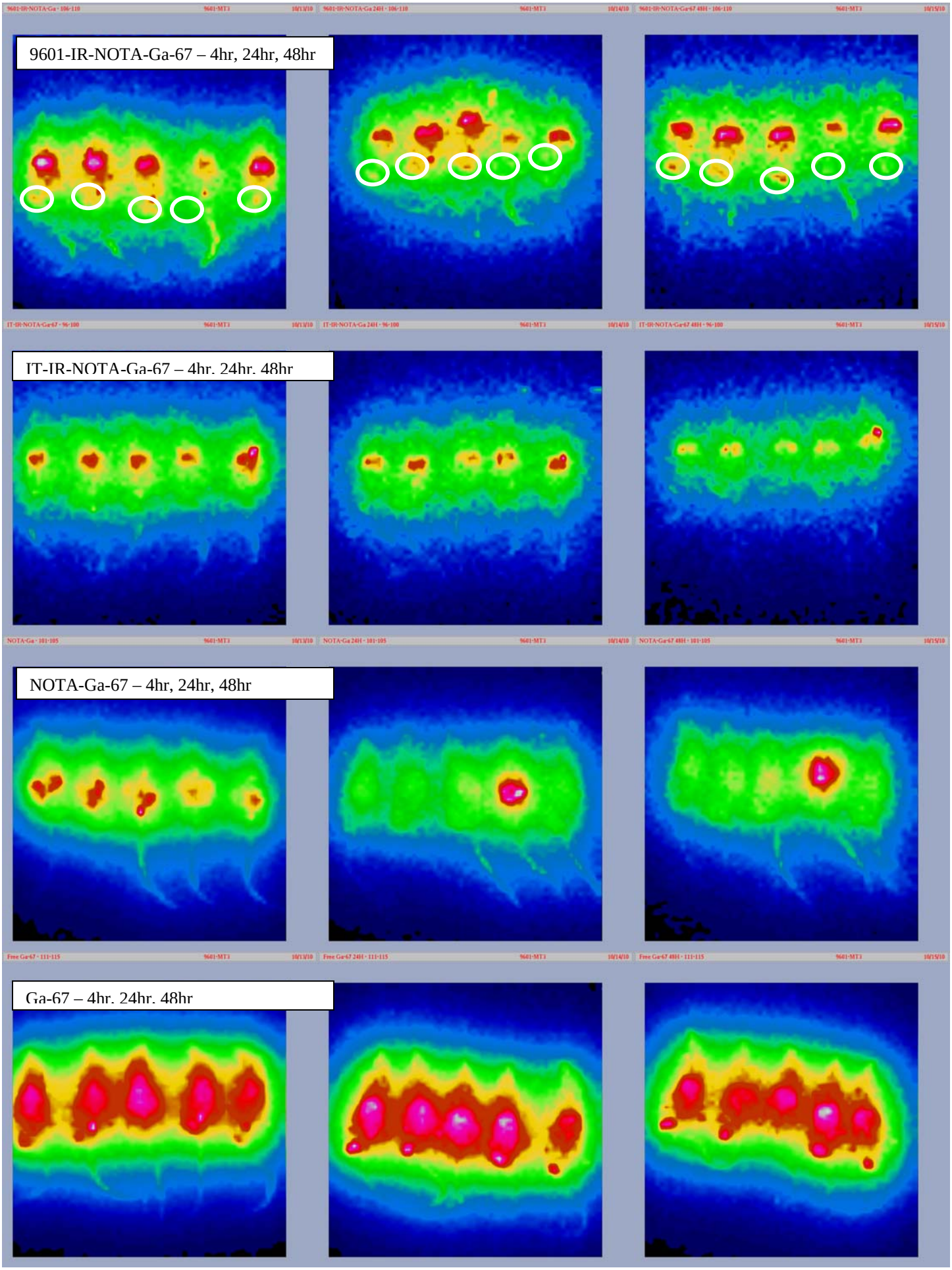
9601-IR-NOTA-Ga-67 – 4hr, 24hr, 48hr
IT-IR-NOTA-Ga-67 – 4hr, 24hr, 48hr
NOTA-Ga-67 – 4hr, 24hr, 48hr
Ga-67 – 4hr, 24hr, 48hr

Figure 22: SPECT images showing uptake of Ga-67 in nude mice with Ep-CAM expressing human xenograft tumors in their right flank (images show anterior view of animals, right flank tumor is on left side of mouse). Top row: 9601-IR-NOTA-Ga-67 4hr, 24hr, 48hr, second row: IT-IR-NOTA-Ga-67 4hr, 24hr, 48hr, third row: NOTA-Ga-67 4hr, 24hr, 48hr, and forth row: Ga-67 4hr, 24hr, 48hr. Ga-67 is clearly present in the tumors in the 9601 mice and the free Ga-67 mice but not in the IT or NOTA-Ga mice.

In addition to SPECT imaging, NIR imaging was done at 24 and 48 hours to determine if the NIR signal is present in the same locations as the Ga-67 signal. The 48 hour whole animal and organ images are presented in figure 23.

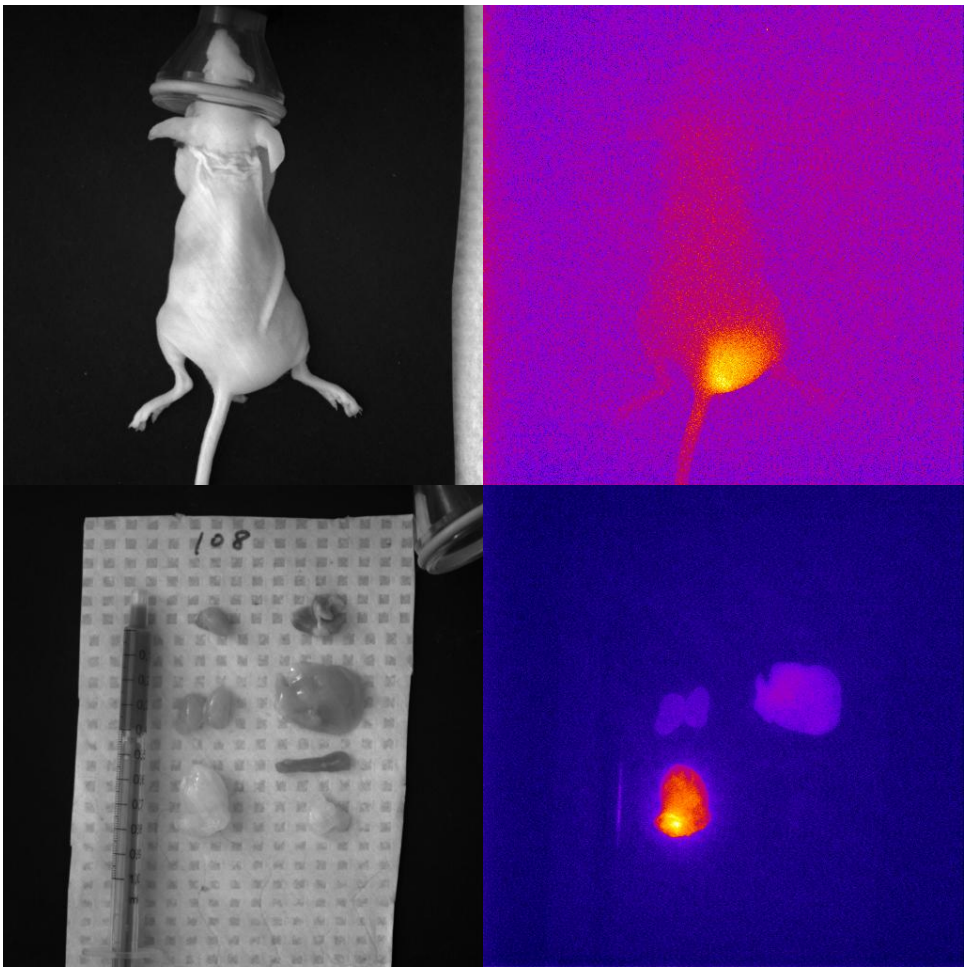

Figure 23: Representative image of a nude mouse from the anti-EpCAM (9601) group at 48 hours and after organ excision, from top right: blood, heart, lungs, row 2: kidneys, liver, row 3: tumor, spleen, and row 4: muscle. The organ with the highest NIR signal was the tumor, as seen both in the whole animal image and the excised organs image.

By defining a region of interest around the tumor region and the contralateral muscle, the fluorescent intensity was determined in the tumor and the background of the mice. Using the same method, the fluorescent intensity was determined in each organ. Figure 24 presents the numerical fluorescence measured from each region of interest, showing that at each time point, the NIR fluorescence was always higher in the tumor than the muscle for the 9601 group, and at each time point, the tumors from the 9601 group always had a higher NIR signal than the tumors from the IT group.

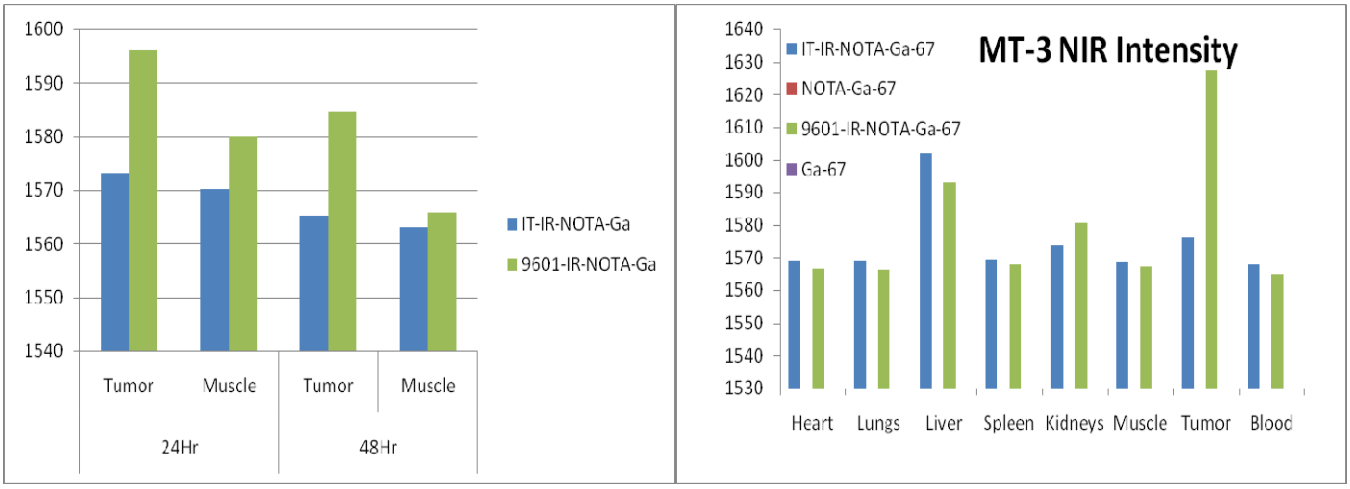

Figure 24: The NIR fluorescent signal from the tumor and muscle regions in the mice who received 9601-IR-NOTA-Ga-67 or IT-IR-NOTA-Ga-67 intravenous injections. The 9601 group showed higher NIR signal in the tumor region than in the muscle region and the 9601 group showed higher NIR signal in the tumor region than the IT group in the whole animal imaging (graph on left) and the excised organ imaging (right).

The preliminary data detailed herein shows that the dual-labeled anti-Ep-CAM antibody 9601-IR-NOTA-Ga-67 results in a higher signal from the tumor than the rest of the animal. Experiments are currently underway to provide the histological evidence that the anti-Ep-CAM is binding to the Ep-CAM expressing tumor and to determine if the agent is present in lymph nodes where metastatic spread of the tumor cells has occurred.

This work suggests that 9601-IR-NOTA-Ga-67 could be a good imaging agent for the detection of Ep-CAM positive tumor cells.

Although higher intensity was present in the left axillary lymph node (tumor positive) than the right axillary lymph node (tumor negative), there was still significant intensity in the negative node. This retention could be due to the Fc receptor present on immune cells in the lymph nodes or due to the large size of the antibody increasing the antibody clearance time.

Phase III of the preclinical anti-Ep-CAM imaging was completed, including the *in vivo* imaging of a dual-labeled anti-Ep-CAM imaging agent, 9601-IR-NOTA-Ga-67. The anti-Ep-CAM agent seemed higher in lymph nodes that were inoculated with breast cancer tumor cells and in subcutaneous tumors, the anti-Ep-CAM agent build up specifically in the Ep-CAM positive tumor rather than the surrounding tissues.

Phase IV of the preclinical anti-Ep-CAM imaging was not included in the SOW originally proposed in this grant application. It was added to the SOW after the move from Baylor College of Medicine to the University of Texas Health Science Center at Houston in response to the previously described difficulties with the anti-Ep-CAM antibody imaging in mice. When this was added, there was no corresponding removal of proposed work.

Phase IV of the preclinical anti-Ep-CAM imaging included generation of anti-Ep-CAM scFv using bacterial and mammalian expression, dual-labeling the scFv, stability studies, binding and blocking studies, generating tumors in mice, in vivo binding and clearance, and biodistribution studies.

To increase the clearance speed of the Ep-CAM binding agent, we are developing smaller binding molecules based upon the antibody. Although whole antibodies, such as trastuzumab (Herceptin) for Her-2 positive cancers, have been used clinically as an anti-cancer therapy [1-5], it may be necessary to utilize a smaller antibody fragment that does not contain the Fc domain to detect metastatic cancer in the lymph nodes. Certain cells within the lymph system such as lymphocytes and NK cells have Fc receptors (FcR) on their surface, and therefore may bind and clear the anti-Ep-CAM antibody before it has a chance to reach the tumor nodules. When these cells bind to the Fc domain of an antibody, they can generate an immune response. Therefore, the

removal of the Fc domain from the anti-Ep-CAM agent could also reduce any immunogenicity that could result due to direct injection of the agent into the lymphatic space.

One method for generating smaller antibody fragments is papain digestion. Anti-Ep-CAM will be digested using papain, a specific thiol-endopeptidase that cleaves an antibody on the amino-terminal side of the disulfide bonds that link the two heavy chains of the molecule. After papain treatment, the original whole antibody will be broken into two Fab fragments and one Fc domain fragment. The Fc fragment can then be removed from the desired Fab product by binding to immobilized Protein A, as schematically described in figure 25.

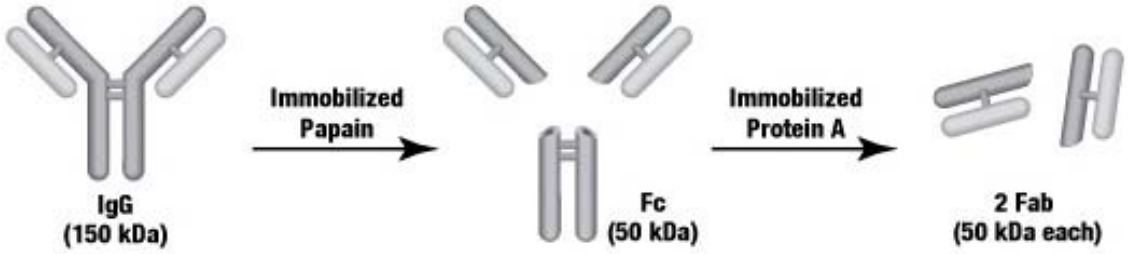

Figure 25: Schematic diagram of Fab generation and purification, image from www.piercenet.com

After papain digestion and purification of the Fab fragments, we will test that the binding functionalities were retained in the Fab after the processing and then the fragments will be dual-labeled and used as Ep-CAM imaging agents in the subsequent experiments. Generating Fab fragments allows testing of an Ep-CAM binding protein with the specific binding ability of the full antibody, but at a third of the size and without the nonspecific Fc domain.

The necessity of removing the Fc domain has not been established, but hopefully, it will improve the agent's ability to bind specifically to tumor cells in the lymph nodes. The Fc receptors (FcR) could bind the full anti-Ep-CAM antibody before it is able to bind the tumor cells, reducing the efficiency of the agent. Binding of the FcR could signal to the immune system to start an immune response, which could have deleterious side effects.

In addition to antibody fragmentation, the binding domain of an antibody can be grafted into a single chain formation called a single chain binding domain (scFv). Initially not all scFvs were stable and functional, but Jung, et al., 1997 reported the ability to graft the binding domain of an antibody onto a known functional single chain variable fragment (scFv) to form a stable scFv directed against any protein of interest.[6] Willuda, et al., 1999, grafted binding domains specific for human Ep-CAM into a stable scFv framework.[7] The amino acid sequences reported in each paper were combined to form the amino acid sequence for the stable anti-hEp-CAM scFv. The resultant amino acid sequence was reverse-translated into a DNA sequence. To the DNA sequence, I added a purification tag (histidine 6) and a cleavage site (enterokinase) to remove the purification tag. The DNA sequence was then codon-optimized for bacterial expression. The resultant DNA sequence was generated and cloned into bacterial expression vectors by DNA2.0 (Menlo Park, CA). The bacterial expression vector will be used to quickly generate large amounts of protein for initial binding and labeling studies.

The scFv gene was cloned into two different bacterial constructs, a vector from Invitrogen, pBAD under control of an L-arabinose promoter, and pJExpress, from DNA2.0, which employed an IPTG promoter. Different strains of E.Coli from New England Biolabs, Qiagen, Invitrogen, and DNA2.0 were used with increasing concentrations of either L-arabinose or IPTG to attempt to express the anti-Ep-CAM scFv to no success.

As an alternative, the scFv was cloned into a mammalian expression vector, pcDNA3. Mammalian expression is generally more difficult than bacterial, but removes any issue of bacterial endotoxin contamination, because proteins expressed in bacteria contain bacterial endotoxins even after purification of the protein of interest. This method also failed to generate the anti-Ep-CAM scFv. Since the expression of the anti-Ep-CAM scFv was not successful after attempts with multiple bacterial expression vectors and bacteria strains nor was it successful

using a mammalian vector and mammalian cells; I concluded that the amino acid sequence I developed from the aforementioned references was missing a vital piece for functional expression.

Thus, an outside company was contracted to use phage display to locate an anti-Ep-CAM scFv from their scFv library. Using a random scFv phage display library, three scFvs specific for Ep-CAM were selected (Creative Biolabs, Shirley, NY). The scFv which showed the highest binding potential when expressed on phage was expressed as a protein and labeled with IRDye 800CW NHS Ester, a near infrared (NIR) fluorescent probe, for detection. At each step in the labeling process, samples were collected, run on a protein gel, and imaged for protein content and NIR fluorescence, as seen in figure 26.

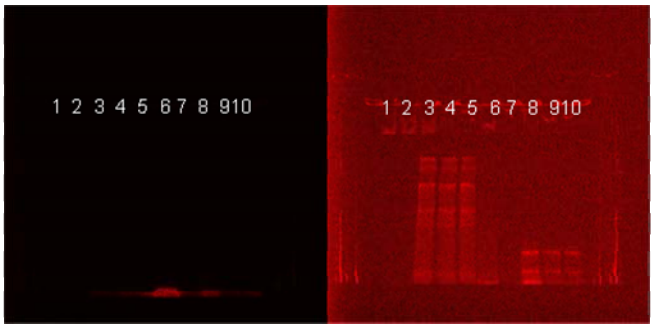

1 – Ladder
2 – Antibody
3 – Antibody + Dye reaction
4 – Antibody-Dye – 1 purification
5 – Antibody-Dye – final purification
6 – Dye
7 – scFv
8 – scFv + Dye reaction
9 – scFv-Dye – 1 purification
10 – scFv-Dye – final purification

Figure 26: NIR fluorescent image of IR800 labeling of anti-Ep-CAM antibody (lanes 3-5) and scFv (lanes 8-10). On the left the image includes the free dye bands at the very bottom of the gel, while on the right, the free dye bands are covered to better image the antibody and scFv bands.

In the initial image (left), the free dye in well 6 oversaturated the camera when using long exposures, so the free dye bands were covered with black paper to get an image (right) of the labeled antibody (wells 3-5) and scFv (wells 8-10). The NIR fluorescence images were collected using our custom-built, small animal imaging system, that contains a near-infrared (NIR) laser, corresponding filters, an image intensifier, a CCD-camera, and a computer.

After successful NIR labeling of the scFv, the binding of the labeled scFv (scFv-NIR) was compared to the binding of the labeled antibody (Ab-NIR). The anti-Ep-CAM agents were incubated with to two breast cancer cell lines, MT-3 (high Ep-CAM expression) and SKBr3 (low Ep-CAM expression) for 1 hour, then the cells were treated with a nuclear stain, cytoxin green (Invitrogen, Carlsbad, CA), mounted on slides and imaged with an upright Leica microscope (Meyer Instruments, Houston, TX). Figure 27 presents overlay images of differential interference contrast (DIC), green fluorescence for nuclear staining (ex 488, em 530), and NIR fluorescence for anti-Ep-CAM staining (ex 785, em 830) images. The DIC images show some 3-dimensional information about the cells for a more complete picture of cell viability.

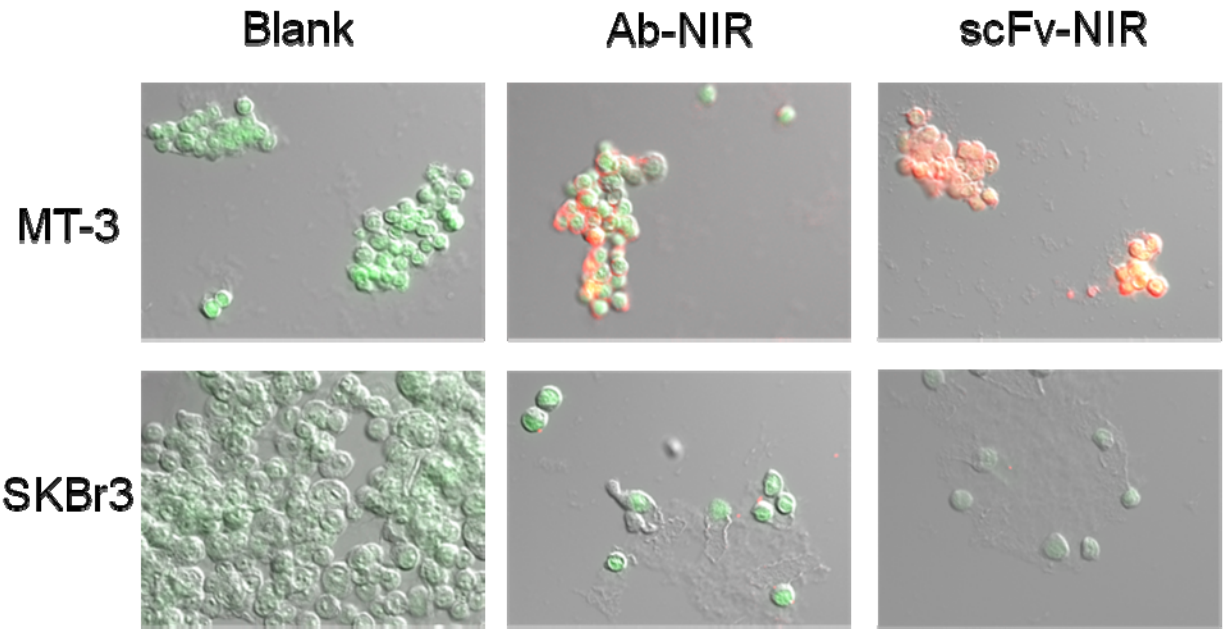

Figure 27: Binding of IRDye 800CW labeled anti-Ep-CAM antibody (Ab-NIR) and scFv (scFv-NIR) to Ep-CAM positive MT-3 cells and Ep-CAM negative, SKBr3 cells. The red pseudocolor represents binding of anti-Ep-CAM agent and green pseudocolor represents cell nuclei.

In these images, sytox-green is a nuclear stain (pseudocolor green) and NIR signal is represented with red pseudocolor. The fluorescent images were overlayed with a white light image of the cells. Both the NIR labeled antibody and scFv bound to the Ep-CAM expressing, MT-3 cells, with very little background binding seen on the SKBr3 cells. The preliminary data suggest that this scFv should be tested in the mouse tumor models.

The two additional scFvs that showed affinity for Ep-CAM during the selection process were also generated in protein form and tested for *in vitro* binding. After IRDye 800CW labeling, microscopy and flow cytometry were used to evaluate their binding properties. Unfortunately the initial successful binding experiments were not repeatable nor did the two additional scFvs generated bind to the Ep-CAM positive cells well, so the decision was made to go back to the initial full length antibody.

Phase IV of the preclinical Ep-CAM Imaging was completed, resulting in the generation of one bacterial expression system for an anti-Ep-CAM scFv, one mammalian expression system of an anti-Ep-CAM scFv, and three anti-Ep-CAM scFvs selected from a phage display library. Unfortunately this did not result in the generation of a scFv capable of binding specifically to Ep-CAM.

Clinical Ep-CAM Imaging Studies

Phase I of the clinical Ep-CAM imaging studies began with observing and learning from Dr. Sevick's clinical trails, learning the steps of IND preparation, and participating in the NIR imaging of the lymphatics of human subjects.

Avoiding the morbidity of lymph node dissection in cancer patients, requires the ability to detect lymph nodes in breast cancer patients after delivery of the cancer detection agent. I was able to observe the proof of principle of imaging an intradermally injected, microdose of NIR fluorescent agents done by our group. Injections of indocyanine green, a NIR fluorophore that is already clinically used, were given intradermally in the distal regions of the arms or legs of subjects and then the subjects were imaged with our clinical imaging cameras that contain a near-infrared (NIR) laser, corresponding filters, an image intensifier, a CCD-camera, and a computer, as shown in Figure 28.

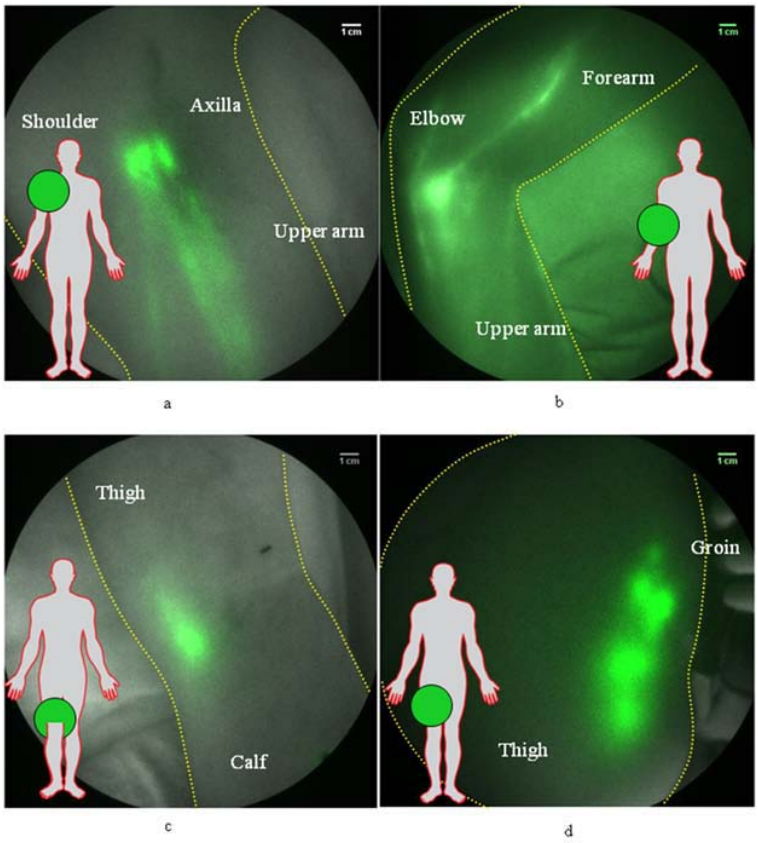

Figure 28: Images of axillary (A), cubital (B), popliteal (C), and inguinal (D) lymph nodes in human subjects after intradermal injection of up to 100 micrograms of indocyanine green.

The ability to detect NIR fluorescence in the lymph nodes of human subjects implies that a NIR labeled agent, such as an anti-Ep-CAM scFv, could be detected in cancer positive lymph nodes in patients. In observing the clinical trials, I have had the opportunity to meet some of the women who are struggling with breast cancer-related lymphedema and the morbidity associated with axillary lymph node dissection. My goal in this work is to improve quality of life for future breast cancer survivors by improving nodal staging with an Ep-CAM targeting agent.

Phase I of the clinical imaging was completed with me learning about the IND submission process and participating in clinical imaging.

Phases II and III of the clinical portion were not initiated. Although some positive results were observed, the data collected did not support the initiation of a clinical trial for this imaging agent.

Instead of the clinical work, more preclinical experiments were designed and initiated.

The entirety of the Phase IV preclinical work was added to the SOW part way through work on the grant with no corresponding removal of down stream tasks. No work was removed because at the time, we thought following the template of work already done for the whole antibody; we would quickly be able to do the same work for a scFv. Unfortunately the design and expression of a scFv specific for Ep-CAM turned out to be a complex process that took more time than anticipated and resulted in the development of 3 scFvs from a phage library that were not significantly specific for Ep-CAM and thus could not be moved forward into human studies.

Work was added to the radiolabeling portion of the dual-labeling of anti-Ep-CAM. Initial work was proposed using DOTA as a chelating agent for Copper 64 and PET imaging. Unfortunately the DOTA chelating reaction required a 95^{o}C heat step, which does not seem to affect the binding of full antibodies, but we were worried would affect the stability and binding of scFvs or other smaller binding molecules. Thus while investigating the use of smaller molecule binding agents, we found a different chelating agent, NOTA was researched which does not require the 95^{o}C heat step. With the use of NOTA, we also moved to using gallium as the radiometal because it is available as Ga-67 (a SPECT agent with a half-life of 3.3 days) and Ga-68 (a PET agent with a half-life of 68 minutes). The long half-life SPECT agent could be used for whole antibody imaging, and the short half live PET agent could be used for imaging of scFvs and other small molecule imaging agents that would clear more quickly from the body. The use of gallium as the radiometal allowed us to develop a single chelating procedure that could result in either a PET or a SPECT agent depending upon the gallium isotope used.

None of the work with the IFP1.4 protein was included in the initial SOW. Initially, we proposed using other fluorescent proteins for the tracking of tumor cells in mice. The discovery of IFP1.4 by Dr. Tsein was very exciting to us because it marked the first time a fluorophore in the near-red region had been developed that could be expressed by human cells. With the discovery of the new fluorophore, we had to build an imaging system capable of measuring IFP1.4 expression with the same sensitivity that our NIR camera allows us to image IRDye 800CW. Using what we learned in building the NIR imaging camera, we built an imaging system for IFP1.4. We started with a 668nm laser diode with a laser line diffuser (30degree) and a laser line clean up filter, which ensures that the incident laser light is within a specified range, for our purposes 670$\pm$10nm. Then on the emission side, we put a bandpass filter, that allows any light >690nm to pass, and a holographic filter, that stops light at 665+15nm from passing, in front of the EMCCD camera lens.

During imaging we noticed that in some frames a significant amount of light leakage was present, as seen in figure 29.

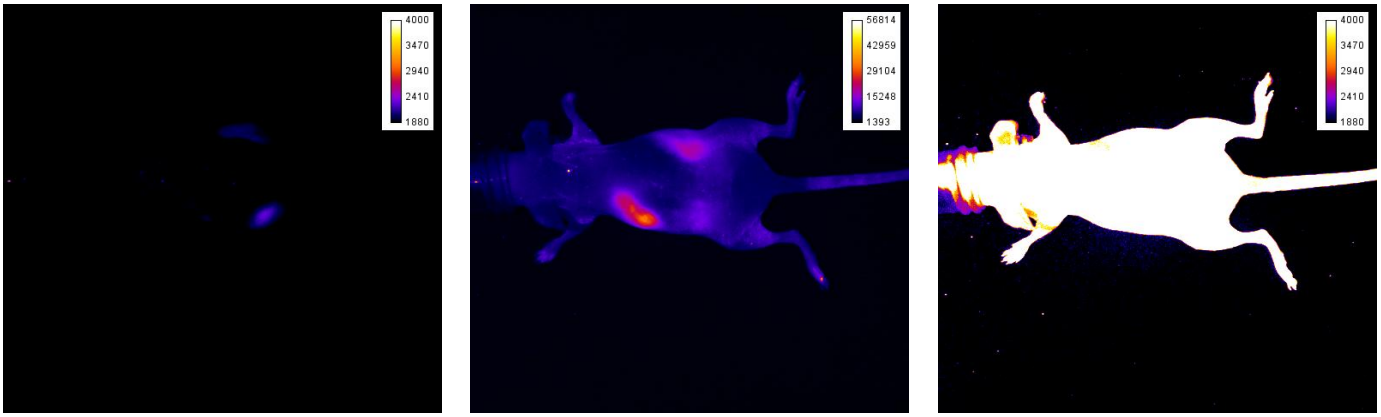

Figure 29: Day 12 images of the dorsal side of nude mice with SKBr3-IFP1.4 tumors. No changes were made in the laser power, filter arrangement, acquisition time, or any other parameter during the imaging.

After investigating, we determined that the temperature controller for the laser diode was not working correctly and the temperature was fluctuating wildly during this imaging session. The laser controller was removed and a different one installed that had more surface area to better disperse the heat. To determine the effect of the changing heat on the system, measurements were taken of the laser beam output over a range of temperatures. The results were graphed and are presented in figure 30.

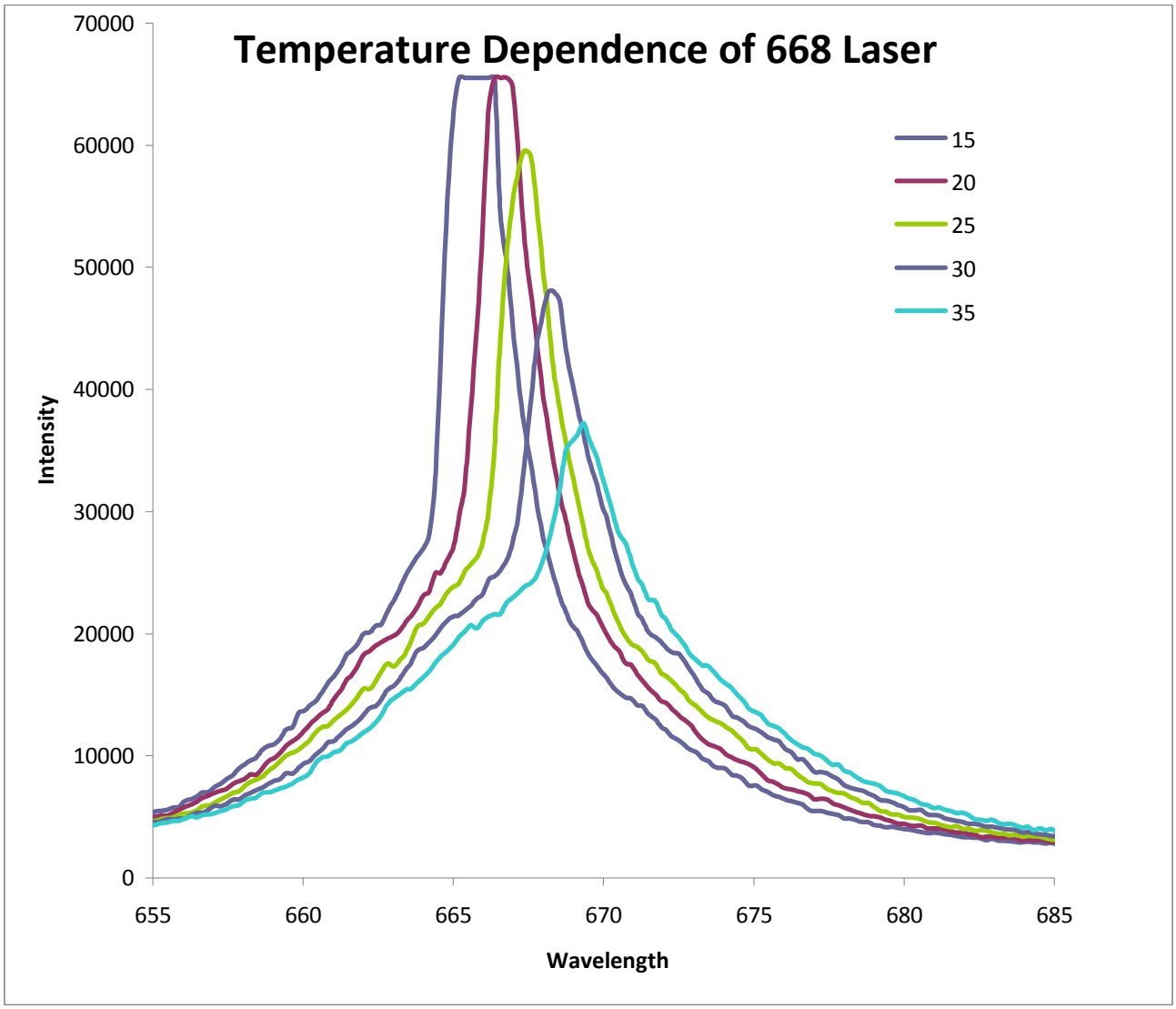

Figure 30: The effect of changing temperature on the laser intensity and wavelength of the 668nm laser at 15, 20, 25, 30 and 35°C. The laser output was measured from 350 to 1050 nm, with only the relevant wavelengths presented in this graph. The operating instructions for the 668nm laser diode specify 25 °C as the optimal temperature for diode performance.

In the graph, it is clear that the laser maximum shifts with temperature and the strength of the beam actually diminishes above the optimal temperature. Although the temperature explains some of the image quality problems seen in figure 29, it does not completely explain the large quality difference seen in the three images. Thus the measurements were repeated using different filter combinations to determine which the effectiveness of the filter sequence. Initial measurements were collected by placing the Ocean Optics probe at the surface of the tissue to determine the incident laser power at the tissue (or mouse) being imaged. The normal imaging set up is described schematically in figure 31.

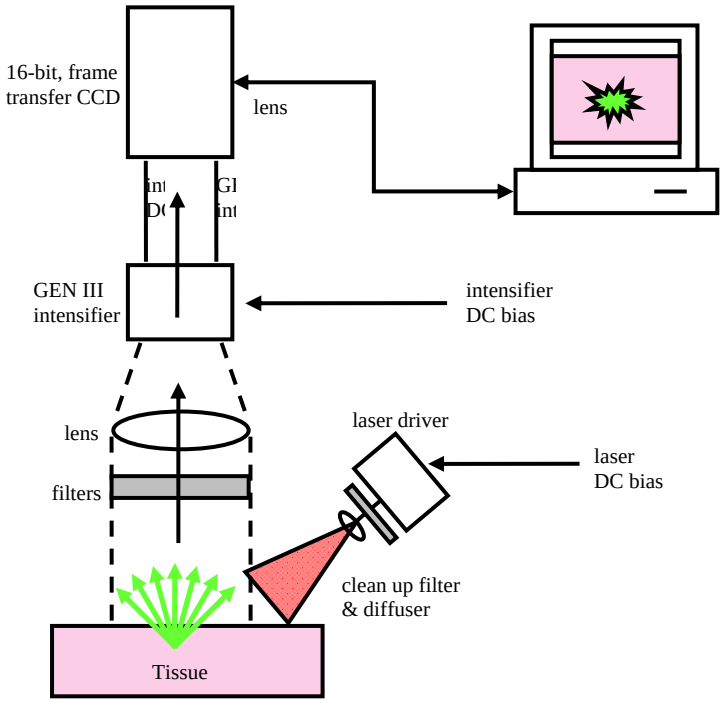

Figure 31: Schematic representation of the optical imaging system used to measure fluorescent signals in mice.

To measure the laser intensity at the surface of the tissue or mouse, this set up was altered, removing the camera and associated filters and using the optical probe to measure the laser output as shown in figure 32.

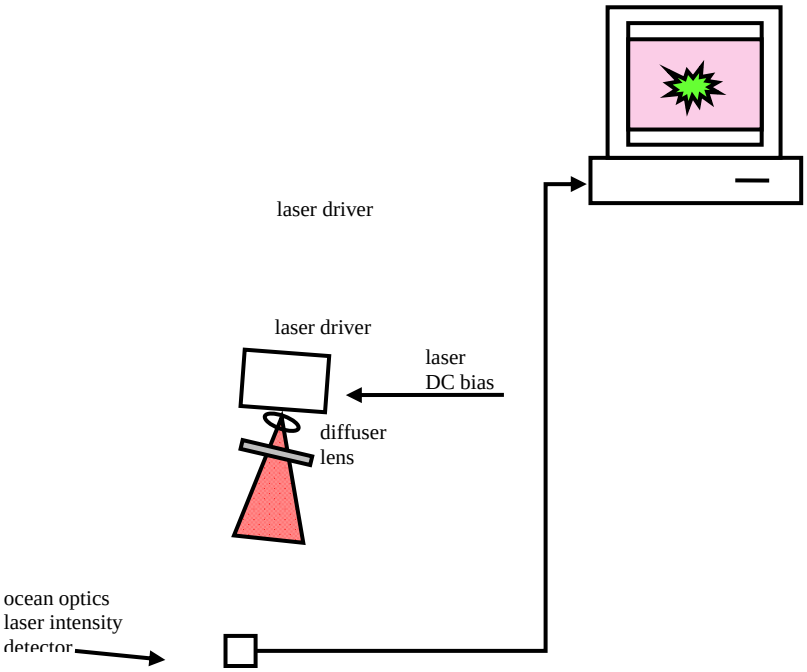

Figure 32: Schematic of laser output measurement set up. The Ocean Optics probe is directly measuring the laser output and sending the measured values to the computer.

With the Ocean Optics probe in place the laser output was measured to determine the effects of the clean up filter and diffuser on the laser line. Figure 33 displays the measured laser intensities.

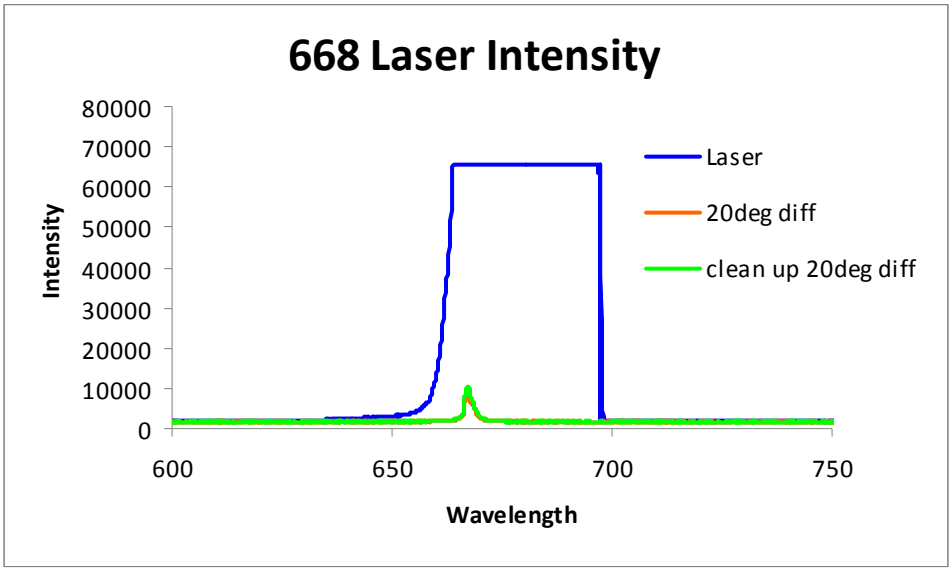

Figure 33: Laser intensity at the tissue surface. The measurement time was extended due to the reduction in laser intensity after the diffuser was placed in front of the laser source. There was little to no reduction in laser intensity measured after the addition of the clean up filter.

This initial measurement reports that the intensity of the laser is reduced at the tissue surface due to the diffusion of the laser line. This diffusion is necessary to cover the entire imaging field evenly with laser light. The laser itself emits a narrow beam of laser light which can excite flourophores in a very small area, but when the goal is to image a larger area, the laser light must be diffused.

After determining that the diffuser and clean up filter were causing laser line or light fluctuations, we moved to measuring the laser intensity after the bandpass and holographic filters but before the camera lens. The set up for these experiments is shown schematically in figure 34.

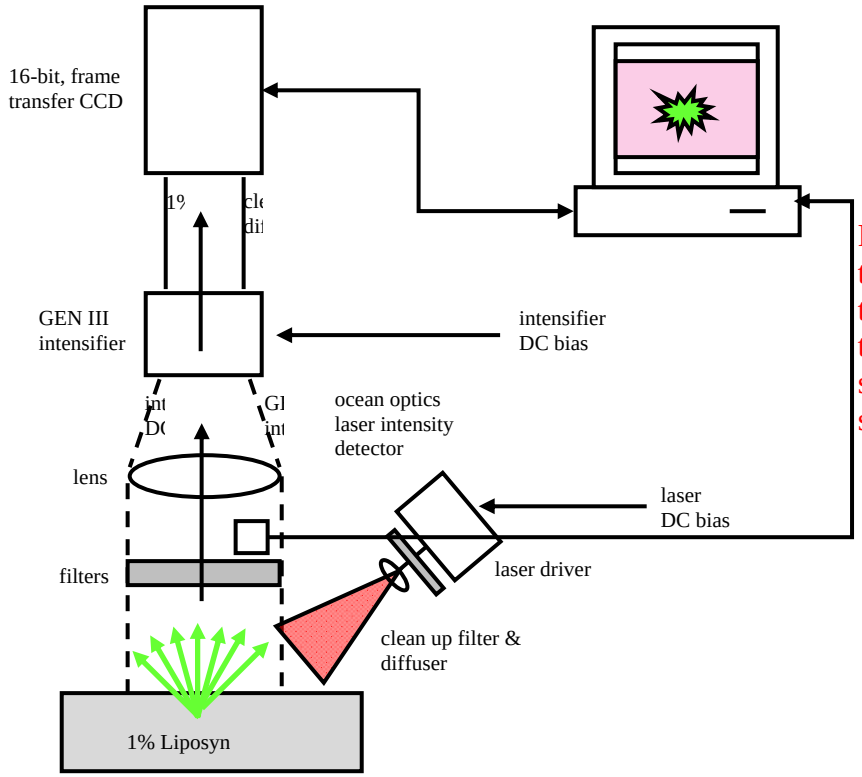

Figure 34: Schematic description of the imaging system set up to measure the laser intensity that passes through the filters after reflecting off the tissue surface, here represented with a liposin solution.

All of the measured intensities include the clean up filters and diffuser on the laser, the data labels describe the filters in front of the camera lens. The measured intensities of the 668nm laser were graphed and are presented in figure 35.

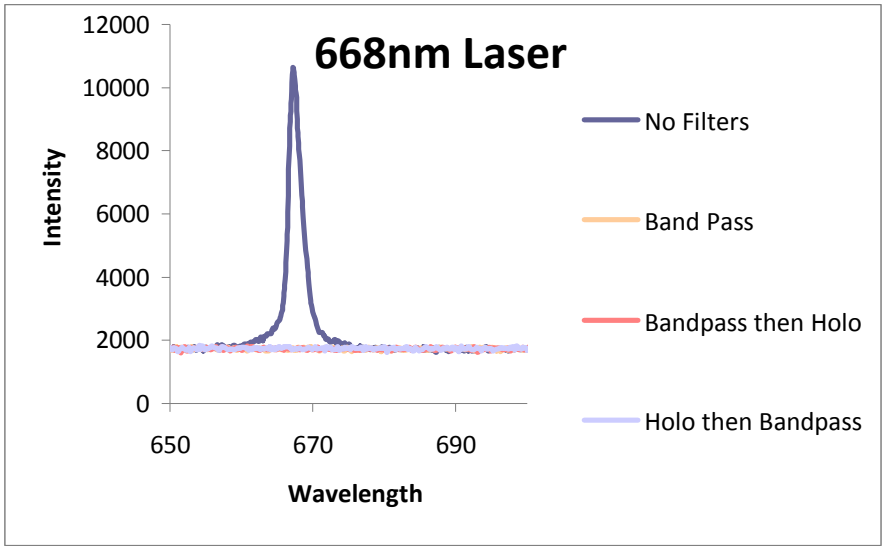

Figure 35: The measured intensities from the 668nm laser in front of the camera lens. In front of the laser there was a diffuser and a clean up filter. The blue line represents the reflected laser intensity with no filters, the yellow line represents only the bandpass filter, the orange line represents the bandpass and then the holographic filter and the purple line represents the holographic filter then the bandpass filter in front of the camera lens.

Although this information tells us that the reflected light from the liposin solution is being filtered properly by our set up of bandpass and then holographic filters, the best measure for camera performance is to measure the transmission ratio. To measure the transmission ratio, the Ocean Optics device is removed and the captured by the camera are recorded. In this experiment, the 1% liposin solution is made and then a serial dilution of a fluorophore is made in the liposin. In this case, our 1% liposin solutions contained 0, 0.001, 0.01, 0.1, 1, or 10 μM Alexafluor 680 (AF680). To determine the intensity measured at the camera, images were taken of each solution in a petri dish. Then a region of interest was selected to include most of the petri dish, but to exclude the rims and accompanying edge effects. Each measurement was taken 3 times and the average value used to determine the transmission ratio. The equation for the transmission ratio is:

$$T_R = \frac{I_{lip}}{I_{fl} - I_{lip}}$$

Where

I_{lip} is the intensity measured from a liposin solution with no fluorophore
I_{fl} is the intensity measured from a liposin solution with fluorophore

Looking at the formula, when the concentration of fluorophore in the liposin approaches zero, the transmission ratio should approach infinity. As the concentration of the AF680 fluorophore increases, the intensity should increase, causing the transmission ratio to approach zero. The measured intensities were converted into transmission ratios and the resulting values were graphed and are displayed in Figure 36.

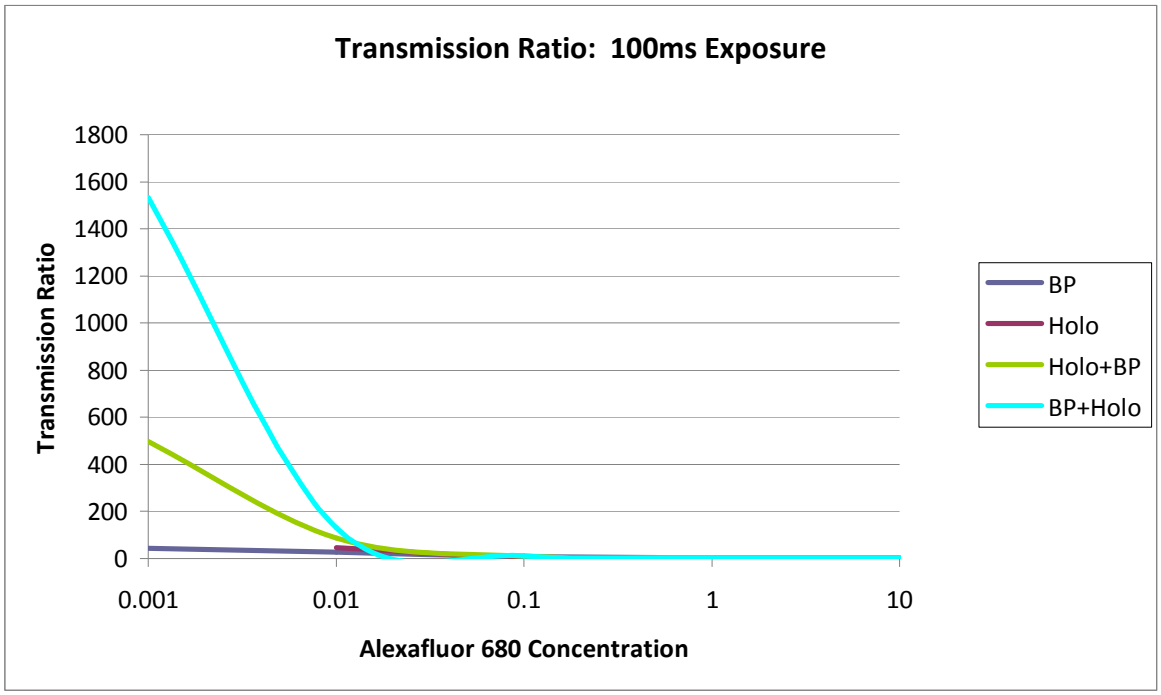

Figure 36: Transmission ratios of different filters for Alexafluor 680 in 1% liposin.

Over the small concentration range of 0.001 to 10 μM AF680 in liposin, the transmission ratio behaves as predicted, decreasing with increasing AF680 concentration and increasing with decreasing AF680 concentration. But interestingly, this relationship does not hold at higher concentrations. As the AF680 concentration increases to 100 or 1000 μM suddenly the tranmission ratio begins to increase again, as shown in Table 4.

	Measured Intensity				Transmission Ratio			
μM AF680	BP	Holo	Holo+BP	BP+Holo	BP	Holo	Holo+BP	BP+Holo
0	1792.93	2563.89	1827.24	1832.49				
0.001	1833.03	2511.43	1830.92	1833.69	44.71		496.89	1533.46
0.01	1858.99	2618.42	1848.23	1846.55	27.14	47.02	87.05	130.38
0.1	2005.72	3598.07	1997.14	1989.59	8.43	2.48	10.75	11.66
1	2988.93	9687.19	2913.53	2962.90	1.50	0.36	1.68	1.62
10	3051.79	10886.48	3022.78	2969.08	1.42	0.31	1.53	1.61
100	1902.89	2734.61	1901.90	1901.34	16.31	15.02	24.47	26.62
1000	1842.50	2078.57	1838.25	1840.68	36.17		165.95	223.68

Table 4: Actual intensity values for the serial dilution of AF680 in liposin, and the resulting transmission ratios.

This interesting phenomenon is due to the signal multiplicative functions of the EMCCD camera. The devices and filters used in our imaging system are designed specifically for the ability to image ultra low concentrations of fluorophore and thus did not function at its best in high concentration cases. In addition, the holographic filter did not effectively block any light as shown in table 4. In every measured case, the holographic filter alone let through the most light. The holographic filter is there specifically to reduce the amount of laser light reflected off the imaged surface that reaches the camera. The data here show that the holographic filter alone is not able to block reflected laser light, but that adding the holographic filter to the bandpass filter did not significantly change the signals detected. Despite this finding, we choose to remove the holographic filter from our IFP1.4 imaging station to reduce the possibility of interference from the filter stacking. The building and validation of the IFP1.4 imaging system allowed us to image IFP1.4 stable cells *in vitro* and *in vivo* for the tracking of tumor growth in mice.

Key Research Accomplishments

Developed dual labeled anti-Ep-CAM agent – anti-Ep-CAM-IR800-NOTA-Ga-67

Anti-Ep-CAM-IR800-NOTA-Ga-67 bound specifically to Ep-CAM positive cells *in vitro.*

Anti-Ep-CAM-IR800-NOTA-Ga-67 was retained in Ep-CAM positive xenograft tumors in mice.

Reportable Outcomes

Development of targeted imaging agent anti-Ep-CAM-IR800-NOTA-Ga-67 which bound to Ep-CAM positive cells *in vitro* and *in vivo* as xenograft tumors.

ADAMS KE and Sevick EM. Detecting Ep-CAM positive metastatses in the lymph nodes. LINKS (Leading Innovative Networking and Knowledge Sharing) meeting, Department of Defense, Washington DC, January 2010.

ADAMS KE and Sevick EM. Imaging of Ep-CAM positive metastatic cancer in the lymph system. HSEMB: Houston Conference on Biomedical Engineering Research, Houston, TX, March 2009.

ADAMS KE and Sevick EM. Detection of Ep-CAM positive cancer in axillary lymph nodes of mice. UT-Inter-Institutional Department of Biomedical Engineering Symposium, January 2009.

ADAMS KE and Sevick EM. Imaging of Ep-CAM positive metastatic cancer in the lymph system. DOD Era of Hope Breast Cancer Meeting, Baltimore, MD, June 2008.

Conclusion

Increasing the speed and accuracy of nodal staging is vital because the majority of cancer mortalities occur due to distant metastases rather than the primary tumor. The lymph system provides a primary route for the spread of metastatic cancer cells, thus lymph node status serves as the primary prognostic indicator in most cancers. Currently, occult lymph node staging is extremely invasive and time consuming, requiring surgical removal of lymph nodes for biopsy. This surgical disruption of the lymphatic system followed by radiation has a significant morbidity. Specifically, for breast cancer, axillary node resection is associated with an elevated risk of breast cancer-related lymphedema.

This work developed an imaging agent, anti-Ep-CAM-IR800-NOTA-Ga-67, both for optical fluorescence imaging and for nuclear imaging. The agent is capable of specific binding to Ep-CAM positive cells *in vitro* and *in vivo* in xenograft tumor models in nude mice. This binding was measured using the nuclear agent, Gallium-67, and the optical agent, IRDye 800. The nuclear imaging is capable of deeper penetration and can be resolved into 3-dimensional information, while the optical imaging is capable of very fast acquisition times and high special resolution 2-dimensional surface information.

References

1. Goel S, Chirgwin J, Francis P, Stuart-Harris R, Dewar J, Mileshkin L, Snyder R, Michael M, and Koczwara B. Rational use of trastuzumab in metastatic and locally advanced breast cancer: implications of recent research. Breast. Epub Dec 21, 2010.

2. Cortes J, Saura C, Bellet M, Munoz-Couselo E, Ramirez-Merino N, Calvo V, Perez J, and Vidal M. Her2 and hormone receptor-positive breast cancer-blocking the right target. Nat Rev Clin Oncol, Epub Dec 14, 2010.

3. Lennon S, Barton C, Banken L, Gianni L, Marty M, Baselga J, and Leyland-Jones B. Utility of serum Her2 extracellular domain assessment in clinical decision making: pooled analysis of four trails of trastuzumab in metastatic breast cancer. J Clin Oncol, Apr 1:27(10):1685-93, 2009.

4. Ma WW and Adiei AA. Novel agents on the horizon for cancer therapy. CA Cancer J Clin. Mar-Apr:59(2):111-37, 2009.

5. Seidenfeld J, Samson DJ, Rothenberg BM, Bonnell CJ, Ziegler KM, and Aronson N. Her2 testing to manage patients with breast cancer or other solid tumors. Evid Rep TEchnol Assess (Full Rep). Nov:(172):1-362, 2008.

6. Jung S and Pluckthun A. Improving in vivo folding and stability of a single-chain Fv antibody fragment by loop grafting. Protein Eng. Aug:10(8)959-66, 1997.

7. Willuda J, Honegger A, Waibel R, Schubiger PA, Stahel R, Zangemeister-Wittke U, Pluckthun A. High thermal stability is essential for tumor targeting of antibody fragments: engineering of a humanized anti-epithelial glycoprotein-2 (epithelial cell adhesion molecule) single-chain Fv fragment. Cancer Res. Nov 15:59(22):5758-67, 1999.

8. Shu X, Royant A, Lin MZ, Aguilera TA, Lev-Ram V, Steinbach PA, and Tsien RY. Mammalian expression of infrared fluorescent proteins engineered from a bacterial phytochrome. Science. May 8:324(5928)804-7, 2009.

9. Shaner NC, Lin MZ, McKeown MR, Steinbach PA, Hazelwood KL, Davidson MW, and Tsien RY. Improving the photostability of bright monomeric orange and red fluorescent proteins. Nat Methods. Jun:5(6):545-51, 2008.

Appendices